Direction Selectivity of Synaptic Potentials in Simple Cells of the Cat Visual Cortex

BHARATHI JAGADEESH,[1] HEIDI SUE WHEAT,[2] LEONID L. KONTSEVICH,[3] CHRISTOPHER W. TYLER,[3] AND DAVID FERSTER[2]

[1]*Laboratory of Neuropsychology, National Institute of Mental Health, National Institutes of Health, Bethesda, Maryland 20892;* [2]*Department of Neurobiology and Physiology, Northwestern University, Evanston, Illinois 60208; and* [3]*Smith-Kettlewell Eye Research Institute, San Francisco, California 94115*

Jagadeesh, Bharathi, Heidi Sue Wheat, Leonid L. Kontsevich, Christopher W. Tyler, and David Ferster. Direction selectivity of synaptic potentials in simple cells of the cat visual cortex. *J. Neurophysiol.* 78: 2772–2789, 1997. The direction selectivity of simple cells in the visual cortex is generated at least in part by nonlinear mechanisms. If a neuron were spatially linear, its responses to moving stimuli could be predicted accurately from linear combinations of its responses to stationary stimuli presented at different positions within the receptive field. In extracellular recordings, this has not been found to be the case. Although the extracellular experiments demonstrate the presence of a nonlinearity, the cellular process underlying the nonlinearity, whether an early synaptic mechanism such as a shunting inhibition or simply the spike threshold at the output, is not known. To differentiate between these possibilities, we have recorded intracellularly from simple cells of the intact cat with the whole cell patch technique. A linear model of direction selectivity was used to analyze the synaptic potentials evoked by stationary sine-wave gratings. The model predicted the responses of cells to moving gratings with considerable accuracy. The degree of direction selectivity and the time course of the responses to moving gratings were both well matched by the model. The direction selectivity of the synaptic potentials was considerably smaller than that of the intracellularly recorded action potential, indicating that a nonlinear mechanism such as threshold enhances the direction selectivity of the cell's output over that of its synaptic inputs. At the input stage, however, the cells apparently sum their synaptic inputs in a highly linear fashion. A more constrained test of linearity of synaptic summation based on principal component analysis was applied to the responses of direction-selective cells to stationary gratings. The analysis confirms that the summation in these cells is highly linear. The principal component analysis is consistent with a model in which direction selectivity in cortical simple cells is generated by only two subunits, each with a different receptive-field position and response time course. The response time course for each of the two subunits is derived for four analyzed cells. Each derived subunit is linear in spatial summation, suggesting that the neurons that comprise each subunit are either geniculate X-cells or receive their primary synaptic input from X-cells. The amplitude of the response of each subunit is linearly related to the contrast of the stimulus. The subunits are nonlinear in the time domain, however: the response to a stationary stimulus whose contrast is modulated sinusoidally in time is nonsinusoidal. The principal component analysis does not exclude models of direction selectivity based on more than two subunits, but such higher-order models would have to include the constraint that the extra subunits form a smooth continuum of interpolation between the properties derived from the two subunit solution.

INTRODUCTION

With the rise of ever more complex computational models of the brain, the question of how individual neurons perform their computational tasks has become increasingly important. Linear neurons hold appeal for the ease with which their computational function can be analyzed. Neurons that combine their inputs in a nonlinear way (prior to threshold) are capable of performing much more complex computations (Koch and Poggio 1992). Some of the most precise measurements of linearity in a neuronal system have been applied to the assembly of receptive fields in the visual system, in part because of the ease with which visual stimuli can be precisely controlled (Shapley and Lennie 1985). Layer 4 of the visual cortex has been of particular interest because it is the site of a radical transformation in the response properties of visual neurons. The simple cells of layer 4 will respond only to stimuli of the proper orientation, size, disparity, and often direction of motion, yet their afferent inputs, the relay cells of the lateral geniculate nucleus (LGN), will respond to a wide variety of visual stimuli by virtue of their circularly symmetric receptive fields. A great number of experiments have focused on the degree to which simple cells resemble linear filters and the degree to which they apply linear operators to their synaptic inputs in constructing their highly selective receptive fields.

The linearity of processing underlying the direction selectivity of simple cells has come under particular scrutiny in the past several years. All motion detectors must somehow compare the image from at least two different visual field locations at two different times. Early models of direction selectivity emphasized nonlinear interactions between the signals from different visual field locations, each of which had different response latencies (Barlow and Levick 1965; Poggio and Reichardt 1973; Reichardt 1961). More general models of motion processing, however, have shown that neurons could, in theory, become direction selective through linear combinations of such signals (Adelson and Bergen 1985; Burr 1981; Burr et al. 1986; Watson and Ahumada 1983, 1985).

Models of direction selectivity in simple cells have developed in parallel with the more general models of direction selectivity. Initial experiments were interpreted as evidence for nonlinear mechanisms of direction selectivity (Bishop et al. 1973; Emerson and Gerstein 1977; Ganz and Felder 1984; Goodwin et al. 1975). Subsequently, Reid et al. (1987,

1991) demonstrated that different parts of the receptive fields of some simple cells differed in the time course of their responses to flashing stimuli, and that these responses when applied to a purely linear model could accurately predict the preferred direction of each cell.

What remains controversial, however, is the degree to which nonlinear mechanisms enhance the output of the initial linear stage, and what the nature of those nonlinear mechanisms might be. Although purely linear models correctly predict the preferred direction and velocity of simple cells, they consistently underestimate the degree of direction selectivity, that is, the difference in the size of the responses to the preferred and nonpreferred direction of motion. Reid et al. (1991), McLean and Palmer (1989), McLean et al. (1994), Albrecht and Geisler (1991) and DeAngelis et al. (1993) found that linear mechanisms account for one-third to one-half of the direction selectivity of simple cells, and they suggest that the remaining portion is accounted for by a stationary and nonspecific nonlinear filter, such as the spike threshold applied to the output of the linear mechanism. A threshold mechanism, for example, could completely suppress the ability of the weaker synaptic potentials evoked by the stimulus of the nonpreferred direction to trigger action potentials, thus generating strongly direction-selective action potentials from moderately direction-selective synaptic potentials. Tolhurst and Dean (1991), however, have argued that linear mechanisms can explain no more than one-fifth of the direction selectivity of simple cells, and that direction selectivity must arise predominately from suppression of the responses to stimuli of the nonpreferred direction by inhibitory synaptic inputs that are themselves direction selective and nonlinear. A third type of nonlinearity, a nonlinear summation of the synaptic potentials of different time course evoked from the different parts of the receptive field (Reid et al. 1991) could also account for the data.

Which of these nonlinear mechanisms are present in simple cells (synaptic inhibition from cells that are already direction selective, nonlinear summation of synaptic potentials with different visual latencies, or nonlinear filtering of the cell's output) is difficult to resolve with experiments based on extracellular recording of action potentials. Extracellular recordings view the synaptic inputs and their integration through the highly nonlinear spike-generating mechanism, which confounds measurement of the linearity of the processes that occur prior to spike initiation. One way to distinguish among the different mechanisms that might underlie the extracellularly observed nonlinearity is to record directly the changes in membrane potential evoked by visual stimuli. In the experiments described in this paper, we have done just that, by measuring intracellularly the responses of simple cells to moving and stationary stimuli. The intracellular measurements were then analyzed using simple linear models for direction selectivity. The linear models were highly successful in predicting each cell's responses to moving stimuli from a linear combination of the responses to stationary stimuli. From this analysis it appears that direction selectivity is dependent on synaptic inputs from different parts of the receptive field with different response latencies, just as predicted by extracellular recordings. These inputs are then summed linearly to yield visually evoked changes in membrane potential that are well-tuned for the direction of stimulus motion. The direction selectivity of these signals is then enhanced by the nonlinear relationship between membrane potential and spike frequency to yield the highly directional signals recorded extracellularly. Some of these results have been reported previously (Jagadeesh et al. 1993; Kontsevich 1995).

METHODS

Details of the experimental preparation are similar to those described in Ferster and Jagadeesh (1992). Briefly, young adult cats were anesthetized with intravenous sodium thiopental and placed in a stereotaxic headholder. Muscle relaxants were given to minimize motion of the eyes, and the animals were artificially respired. Whole cell patch recordings in the current-clamp mode were obtained from neurons of area 17 of the visual cortex using the technique developed for brain slices by Blanton et al. (1989). Electrodes were filled with a K^+-gluconate or Cs^+-methanesulfonate solution including Ca^{2+} buffers, pH buffers, and cyclic nucleotides. A tungsten electrode placed in the LGN ipsilateral to the cortical recording electrode was used to evoke field potentials in the cortex. The characteristic differences in the field potentials evoked in different cortical layers were used as a guide in preferentially recording from neurons in layers 3 and 4. The actual laminar position of each cell was identified by the cell's receptive-field properties as well as its intracellular responses to geniculate stimulation, including ortho- and antidromic responses (Ferster and Lindström 1983). Resting membrane potentials ranged from −70 to −45 mV. Input resistance ranged between 70 and 250 MΩ.

Optics and visual stimulation

Phenylephrine hydrochloride (10%) was applied to the eyes to retract the nictitating membranes; atropine sulfate (1%) was applied to dilate the pupils and paralyze accommodation. Contact lenses with 4-mm-diam artificial pupils were inserted. Position and preferred orientation of receptive fields were first characterized with moving bars of light projected onto a tangent screen with a hand-held projector or with a computer-controlled optic bench. Sine-wave gratings were displayed on a Tektronix 608 oscilloscope screen using a Picasso stimulus generator (Innisfree, Cambridge, MA). The grating orientation, spatial frequency, and length were adjusted to match those preferred by the cell under study (although some cells were also tested at other spatial frequencies). The temporal frequency of both the contrast-modulated stationary gratings and the drifting gratings ranged from 1 to 8 Hz. The peak contrast ranged from 16 to 64% and the mean luminance was 20 cd/m^2.

For later application to the linear models, gratings of optimal temporal and spatial frequency, orientation and length, were first drifted in the two directions. For each direction, 4 s of drift were preceded by a $\frac{1}{2}$-s period during which the grating remained stationary. Stationary gratings were presented at eight different spatial phases, spaced at 22.5° intervals between 0 and 157.5°. (The full cycle of 360° was not presented since stationary gratings 180° apart in spatial phase are identical to gratings of the same spatial phase but shifted 180° in temporal phase.) At each spatial phase in turn, 4 s of the stationary grating were presented, preceded by a $\frac{1}{2}$-s period during which the screen was maintained at the mean luminance. Each set of two directions of motion, and of eight spatial phases was repeated up to eight times for a given temporal frequency. Visually evoked responses were low-pass filtered and digitized at 4 kHz and stored by computer. Electrically evoked responses were digitized at 15 kHz.

Median filter

For the analysis described below, only the synaptic potentials evoked by visual stimulation are of interest. When the responses

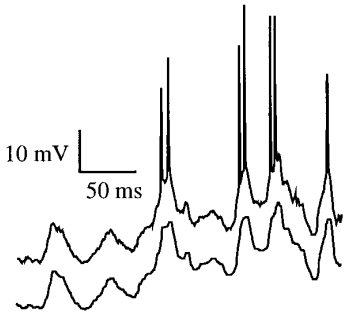

FIG. 1. Median filtering of responses to remove action potentials. *Top trace*: a brief intracellular record from a cortical neuron recorded during visual stimulation with a moving bar. *Bottom trace*: a median-filtered version of the *top trace.* Each digitized point of the *top trace* has been replaced with the median of itself plus the 20 values surrounding it. The effect is to remove action potentials, while leaving the smaller and slower fluctuations in membrane potential largely unchanged.

to 30 or 40 cycles of an optimal grating stimulus are averaged together, however, the numerous and asynchronous action potentials present in the records can distort the apparent shape of the underlying synaptic potentials. Action potentials were therefore removed from the records using a median filter. Before averaging, each digitized point was replaced with the median of itself together with the 20 surrounding values. This algorithm changes the shape of the records little except to remove large transients of a duration shorter than $\frac{1}{2}$ of the 21-point (5 ms) filter width. When the potential monotonically rises or falls during a given 5-ms period, the median will be identical to the original digitized value. For a point within an action potential, however, the median is a value close to the base membrane potential from which the action potential rises since the action potential is far shorter than one-half of the 5-ms filter width. The effect of the median filter on a typical intracellular record is shown in Fig. 1. The spikes in the upper trace have been removed by the filter in the lower trace, but the smaller fluctuations in membrane potential are unchanged except for some of the finest details. All records shown in the figures have been median filtered before display or averaging. The filter had no effect on the results of the analysis of linearity described in this paper.

Analysis of linearity

The main object of the experiment is to determine whether simple cells sum their synaptic inputs linearly in generating their responses to moving stimuli, in other words, whether a cell's response to two stimuli presented simultaneously equals the sum of its responses to the two stimuli presented individually. For example, if the cell is linear, then

$$\mathbf{R}(S_1 + S_2) = \mathbf{R}(S_1) + \mathbf{R}(S_2) \quad (1)$$

where $\mathbf{R}(S_1)$ and $\mathbf{R}(S_2)$ are the responses to the two visual stimuli, S_1 and S_2, presented individually, and $\mathbf{R}(S_1 + S_2)$ the response to the two stimuli presented together. In this case, eight individual stimuli are used, the eight stationary gratings of different spatial phases. Since their sum is a drifting grating, D, as shown in APPENDIX A, *Eq. 1* becomes in this specific case

$$\mathbf{R}(D) = \mathbf{R}(S_1 + S_2 + \cdots + S_8) = \mathbf{R}(S_1) + \mathbf{R}(S_2) + \cdots + \mathbf{R}(S_8)$$

Linearity of spatial summation is not violated, then, if the cell's response to a drifting grating can be expressed as the sum of the cell's responses to stationary gratings of the same contrast, orientation, temporal frequency, and spatial frequency.

Direction index

For a drifting grating, the direction index was defined as

$$\mathrm{DI} = (R_{\mathrm{pref}} - R_{\mathrm{null}})/(R_{\mathrm{pref}} + R_{\mathrm{null}}) \quad (2)$$

where R_{pref}, the response to the preferred direction, is the larger of the responses to the two directions of motion (Reid et al. 1991). For the intracellular experiments, R_{pref} and R_{null} were defined as the peak-to-peak amplitude of the modulation of the membrane potential evoked by the drifting grating moving in the two directions. The direction index for modeled responses to drifting gratings was calculated in a similar way, but preferred and null directions were defined not by which of the modeled responses was larger, but by which of the cell's measured responses was larger (Reid et al. 1991). For a cell preferring upward motion, for example, if the model incorrectly predicted the response to downward motion to be larger, the model's DI would be less than zero.

RESULTS

Nondirectional simple cell

Extracellular recordings have shown that simple cells with spatiotemporally separable receptive fields (that is, cells in which the time course of the response to a stationary stimulus is independent of the stimulus position) are unselective for the direction of motion of a moving stimulus (Albrecht and Geisler 1991; DeAngelis et al. 1993; Emerson and Citron 1992; McLean et al. 1994; Reid et al. 1987, 1991; Tolhurst and Dean 1991). The same is true for simple cells when the receptive fields are defined by intracellularly recorded fluctuations in membrane potential rather than by changes in firing rates. An example of a simple cell with weak direction selectivity is shown in Fig. 2. The averaged responses of the cell to a bar of optimal orientation moving in two directions are comparable in amplitude (Fig. 2*A*). These records also reveal the structure of the cell's receptive field, which was made up of two subregions. As the bar moved to the right, it evoked a depolarization first as it entered the ON region, and then as it left the OFF region. In the reverse direction, a large depolarization was evoked when the bar simultaneously entered the ON region and left the OFF region. (Note that for this and other cells, receptive fields and stimuli are drawn with vertical orientation for simplicity, although in reality preferred orientations varied from cell to cell, as expected.) As do most simple cells (Ferster and Lindström 1983), this cell received monosynaptic excitation from the LGN, as indicated by the short-latency excitatory postsynaptic potential evoked by electrical stimulation of the LGN (Fig. 2*B*). From the shape of this response, and from the depth within the cortex from which the cell was recorded, it is likely that this cell was located in layer 4.

The simple cell of Fig. 2 was insensitive to the direction of motion in response to drifting gratings as well as to moving bars (Fig. 2, *C* and *D*). In Fig. 2*C* are shown the responses to several cycles of drift for the two directions of motion, as indicated in the *insets*. Figure 2*D* contains averages of 21 cycles of the responses to each direction of drift. Two cycles of each averaged response are shown side by side for clarity. The approximately sinusoidal modulation results from the successive activation of the ON and OFF subunits within the cell's receptive field. The

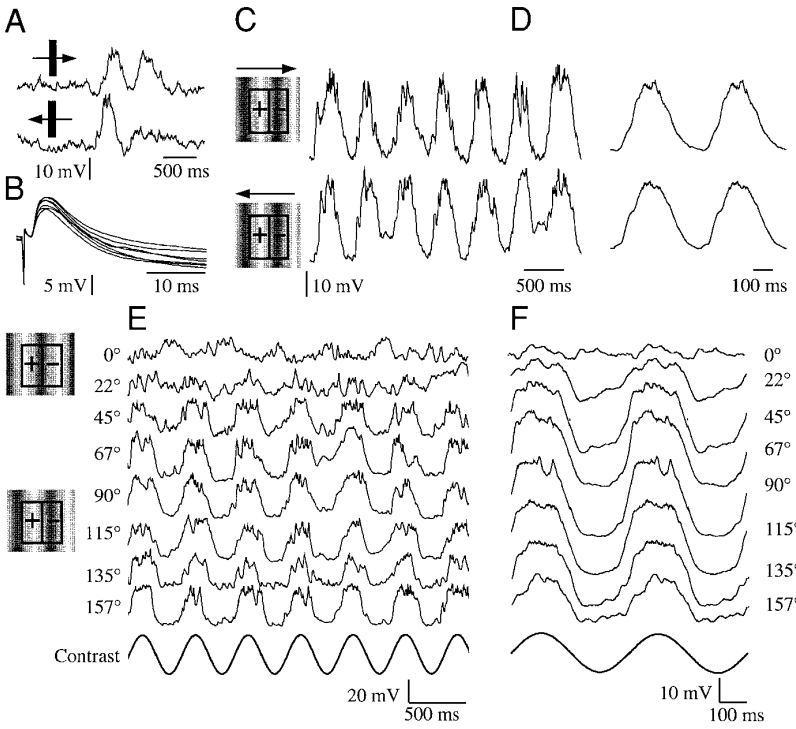

FIG. 2. Intracellularly recorded response of a nondirectional simple cell. *A*: responses to an optimally oriented bar of light sweeping across the cell's receptive field at 10°/s in the direction shown by the arrows. Five individual responses were averaged to obtain the traces shown. *B*: response of the same cell to 1 mA electrical stimulation of the lateral geniculate nucleus at 1 Hz. *C*: responses to sinusoidal gratings drifting across the receptive field at a temporal frequency of 2 Hz. As in all figures, gratings were of optimal spatial frequency and orientation and were presented monocularly to the dominant eye. *D*: averages of 21 cycles of the responses to the 2 directions of motion. Two cycles of the averaged responses are shown side by side. *E*: individual responses to stationary sinusoidally contrast-modulated gratings at 8 different spatial phases (see METHODS). *F*: averages of 21 cycles of the responses to gratings of the same 8 spatial phases. Two cycles of the averaged responses are shown side by side. At the *bottom* of each column is shown the time course of the change in stimulus contrast. *Insets*: approximate position of the gratings at 0 and 90° spatial phase superimposed on the receptive field.

peak of the response occurs as the bright bars enter the ON region and as the dark bars simultaneously enter the OFF region. The minimum of the response occurs when the bright bars enter the OFF region and the dark bars enter the ON region. Although the membrane potential is modulated both above and below rest by the visual stimulus, most of the response carried the membrane potential above the resting potential (as in Fig. 2*A*), suggesting that the response was mediated in large part by increases in synaptic excitation. It is impossible to determine the exact relative contributions of excitation and inhibition, however, simply by examining records taken at a single level of polarization, since the reversal potential of the inhibitory synapses relative to rest was not determined in this cell (Ferster and Lindström 1983). The repolarization that occurs at the end of each peak, however, is likely to represent both a reduction in excitation and an increase in inhibition (Ferster 1988; Heggelund 1986; Palmer and Davis 1981).

The averaged records of Fig. 2*D* allow a precise measurement of the cell's direction index. The peak-to-peak amplitude of the response to rightward motion of the grating was 29.7 mV, whereas the amplitude of the response to leftward (nonpreferred) motion was 28.2 mV. By *Eq. 2*, the direction index for this cell, calculated from the modulations of the membrane potential, was 0.03, which makes this cell one of the least direction selective in our sample.

Response to stationary visual stimuli

Responses of the same cell to stationary, contrast-modulated gratings are shown in Fig. 2, *E* and *F*. The grating was presented at eight spatial phases evenly spaced between 0 and 157°. The temporal and spatial frequency, orientation, and maximum contrast of the stationary grating matched those of the drifting gratings. Individual responses to several cycles of the stimulus are shown in Fig. 2*E;* the average of 21 cycles of the response to each spatial phase are shown in Fig. 2*F*. Two temporal cycles of the averaged responses are shown repeated side by side.

Similar to what has been described in extracellular recordings (Movshon et al. 1978; Reid et al. 1987, 1991), the amplitude of the intracellularly recorded response to the stationary grating depended critically on the position of the grating. For a neuron whose responses are completely space-time separable, the relationship between response amplitude and spatial phase should be a fully rectified sine wave, with a clearly defined null point at which the response amplitude falls to zero. The responses of Fig. 2*F* closely approximate this relationship, as shown in Fig. 3*A*, where the amplitude of the first harmonic of each response in Fig. 2*F* is plotted against spatial phase. The first eight points of the plot are the amplitudes of the first harmonic (2 Hz) components of the traces in Fig. 2*F*. The second eight points are a repetition of the first eight, since the response to a grating presented at $n° + 180°$ of spatial phase will equal the response to a grating at stimulus $n°$, shifted 180° in temporal phase.

Although the amplitude of the response to a stationary grating changes significantly with spatial phase in Fig. 2*F*, the shape of the response changes little. Accordingly, the temporal phase of the first harmonic of the response changes little with spatial phase, as shown in Fig. 3*B*. Between the null points at 0 and 180°, the temporal phase is nearly constant except for a very slight upward trend, which reflects a small but systematic variation in the rising phase of the responses in Fig. 2*F*. Plots of amplitude and temporal phase against spatial phase and of amplitude against temporal phase are shown for a second nondirectional cell in Fig. 3, *D*–*F*. The responses of this cell are shown in Fig. 12*G* and in Fig. 3 of Jagadeesh et al. (1993).

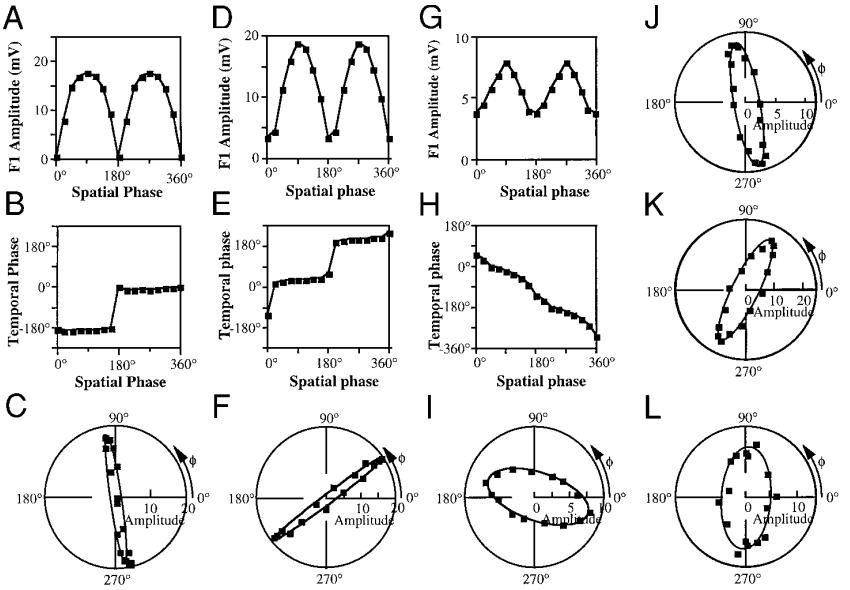

FIG. 3. *A*: amplitude of the 1st harmonic (2-Hz component) of the responses in Fig. 2*F* plotted against the spatial phase of the stimulus. The points between 0 and 180° are repeated between 180 and 360°. *B*: temporal phase of the 1st harmonic of the responses in Fig. 2*F* plotted against the spatial phase of the stimulus. *C*: polar plot of the amplitude of the 1st harmonic of the responses in Fig. 2*F* (distance from the origin) plotted against temporal phase (angle from the *x*-axis) for comparison with extracellular data of Reid et al. (1991). An ellipse has been fit to the points with a least-squares algorithm. The ratio of the ellipse axes (0.07) accurately matches the cell's direction selectivity as predicted by Reid et al. (1991). *D–F*: the 3 plots of *A–C* for a 2nd nondirectional simple cell with a direction index of 0.05 (see Fig. 12*G*) (see also Fig. 3 of Jagadeesh et al. 1993). *G–I*: the 3 plots of *A–C* for the directional simple cell of Fig. 5. *J–L*: amplitude plotted against temporal phase for 3 other direction-selective cells.

Modeling direction selectivity

If the neuron illustrated in Fig. 2 is linear in the summation of its synaptic inputs, and if those inputs are linear in spatial summation, then it should be possible to predict the responses of the cell to moving gratings (Fig. 2*D*) from its responses to stationary gratings (Fig. 2*F*). As shown in METHODS and in the APPENDIX, because the drifting gratings are physically equivalent to the sum of the stationary gratings, a linear cell's response to the drifting grating must be equal to the response to the sum of the stationary gratings

$$\mathbf{R}(\text{drifting grating}) = \frac{1}{4}\mathbf{R}\left(\sum_{n=1}^{8} \text{stationary gratings}\right)$$

$$= \frac{1}{4}\sum_{n=1}^{8} \mathbf{R}(\text{stationary gratings})$$

To predict the response to a drifting grating, then, the eight individual responses of Fig. 2*F* must be summed and then divided by 4. As outlined in the APPENDIX, however, the eight stationary gratings must have different spatial phases and different temporal phases (Reid et al. 1991). To be exact, the temporal phase of each component stimulus grating must be equal to its relative spatial phase. Because the responses in Fig. 2*F* were evoked by gratings of different spatial phases but identical temporal phases, before summing the traces to arrive at the predicted response to the drifting grating, each trace must be shifted in temporal phase by an amount equal to the spatial phase of the corresponding grating stimulus. Advances in temporal phase are required to simulate the response to a grating drifting in one direction; temporal delays simulate the response to the other direction.

The appropriate shifts in temporal phase have been made in Fig. 4*A*, where one cycle of each shifted response is shown. On the *left*, temporal delays simulate motion to the right; on the *right*, temporal advances simulate motion to the left. The shifts bring the peaks of some of the traces into line with the troughs of other traces. Because the individual traces are nearly identical in time course, the relationship between the peaks and troughs is nearly the same regardless of whether the traces are shifted left or right. As a result, the sums of the two columns are nearly identical to one another (Fig. 4*B*, thin traces). For comparison, the heavy traces in Fig. 4*B* show the actual responses to drifting gratings taken from Fig. 2*D*. Although the absolute amplitudes of the modeled responses to the drifting gratings are somewhat larger than the actual responses, the model correctly predicts that the cell is not direction selective (predicted direction index: 0.02). The model also predicts the overall shape of the responses to drifting gratings, including the relative timing of the peaks and troughs.

A second method of predicting the direction selectivity of a cell from its responses to stationary visual stimuli was developed by Reid et al. (1987, 1991). These authors measured the amplitude and temporal phase of the first harmonics of extracellular responses to the gratings and plotted them in polar coordinates. The ratio of the minor and major axes of the resulting ellipse was then taken to be a linear prediction of the direction index of the cell. This method of linear prediction is similar to the one used in Fig. 4 except that it is based entirely on the first harmonics of the responses to stationary gratings. The model used in Fig. 4 incorporates the full time course of the stationary responses. A polar plot of phase and amplitude is shown for the simple cell in Fig. 3*C*. The ellipse fit to the data with a least-squares technique is also shown, and the points do conform well to the ellipse. The ratio of the ellipse axes, 0.07, is similar to the direction selectivity predicted by the model presented in Fig. 4. The agreement between the ellipse method and the summation method of Fig. 4 was generally quite high for all recorded cells. Phase plots for a second nondirectional cell (direction index 0.05) are shown in Fig. 3, *D–F*. The same features as are present in the graphs of *A–C* are present.

Responses of a direction-selective simple cell

The responses to drifting gratings of the direction-selective simple cell in Fig. 5 differ markedly from those of the nondirectional cell of Figs. 2–4. Individual responses to the drifting gratings are shown in Fig. 5*A*, and averaged re-

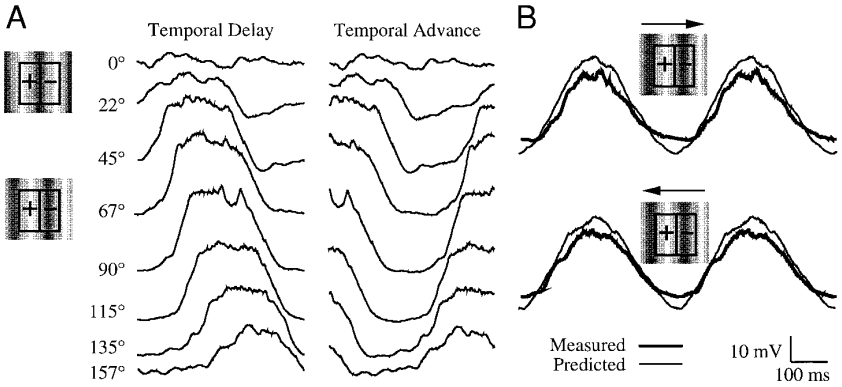

FIG. 4. Application of the data in Fig. 2*F* to a linear model for the prediction of direction selectivity. *A*: averaged responses to stationary gratings shifted in temporal phase by an amount equal to the spatial phase of the corresponding stimulus. *Left column*: each successive trace has been shifted to the right (temporal delay) to simulate motion to the right. *Right column*: each trace has been shifted to the left (temporal advance) to simulate motion to the left. *B*: thin traces are the sums of the 2 columns in *A* reduced in size by a factor of 4 (see APPENDIX A*1*) and are the predictions of the linear model for the response of the cell to gratings drifting in the 2 directions of motion. Thick traces show the actual response of the cell to the drifting gratings (taken from Fig. 2*D*).

sponses in *B*. Not only do the responses to the two directions of motion differ in size from each other, they also differ in shape. Unlike the traces in Fig. 2*D*, the rise and fall of the membrane potential about the peak is asymmetric; the rise to the peak takes a shorter time than the fall to the minimum. This asymmetry is more pronounced in the response to the nonpreferred direction of motion, which resembles a sawtooth. The nearly 3:1 difference in the peak-to-peak amplitudes of the preferred and nonpreferred responses gives this neuron a direction index of 0.40 when measured on the basis of modulations in membrane potential. When measured on the basis of action potentials, this cell had a direction index of 1, because no spikes were elicited by gratings of the nonpreferred direction.

The difference between the direction-selective and non–direction-selective cells is even more striking in their responses to stationary gratings (compare Figs. 2*F* and 5*D*). *1*) For the nondirectional cell, the responses to the stationary gratings at different spatial phases differed in size by more than a factor of 5; for the directional cell, the response amplitude changed only by a factor of 2 with spatial phase. *2*) As has been shown in extracellular recordings (Movshon et al. 1978; Reid et al. 1987, 1991), there is no true null-point for the direction-selective cell. The spatial phase at which the minimum response was evoked has been defined as 0°, but there was a significant response even at this phase. *3*) For the nondirectional cell, each response was similar in shape. For the directional cell, the response shape changed dramatically with spatial phase. At 0° spatial phase, the response was nearly sinusoidal with a gradual rise and fall in membrane potential. Between 45 and 90°, the membrane potential rose very rapidly to a peak and then fell more gradually in two separate stages. As a result, the time of the response peak relative to the stimulus changed by >100 ms between 0 and 90° spatial phase.

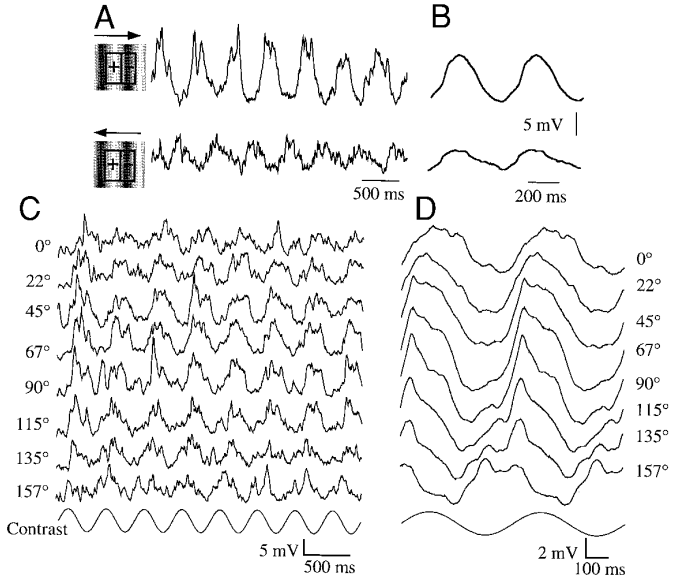

FIG. 5. Response of a directional simple cell to drifting gratings. *A*: individual responses to the preferred (above) and nonpreferred (below) direction of motion. *B*: averaged traces with 2 cycles of the average repeated. *C*: individual responses to sinusoidally contrast-modulated stationary grating of 8 different spatial phases. *D*: averaged traces. At the *bottom* of each column is shown the time course of the change in stimulus contrast.

The dependence on spatial phase of the size and shape of the responses to stationary gratings is shown quantitatively in Fig. 3, *G* and *H*. Compared with the plots of Fig. 3, *A* and *B*, the amplitude of the response is modulated less strongly with changes in spatial phase, and the temporal phase of the response changes more smoothly with spatial phase. The dependence of response shape on spatial phase shown in Fig. 3*H* is exactly analogous to that observed extracellularly in simple cells described by Movshon et al. (1978) and in direction-selective simple cells by Reid et al. (1987, 1991). It should be noted, however, that the amplitude and phase plots of Fig. 3 are derived solely from the first harmonic (2 Hz) of the responses. Although the higher harmonics also change from trace to trace, as reflected in the changing time course of the responses, these changes do not appear in Fig. 3.

The linear model accurately predicts the direction selectivity of the cell of Fig. 5. As in the previously described cell, modeling the responses to drifting gratings requires shifting the responses to stationary gratings in temporal phase, with temporal delays simulating motion in the preferred direction (Fig. 6*A*, *left column*) and temporal advances simulating motion in the nonpreferred direction (*right column*). As shown in the extracellular studies of direction selectivity (Albrecht and Geisler 1991; DeAngelis et al. 1993; Emerson and Citron 1992; McLean and Palmer 1989; McLean et al. 1994; Tolhurst and Dean 1991), the change of the response time course with spatial phase predicts the preferred direction of the cell. In the *left column* of Fig. 6*A*, the temporal shifts bring the peaks of the eight traces into near alignment, whereas in the *right column* the temporal shifts distribute

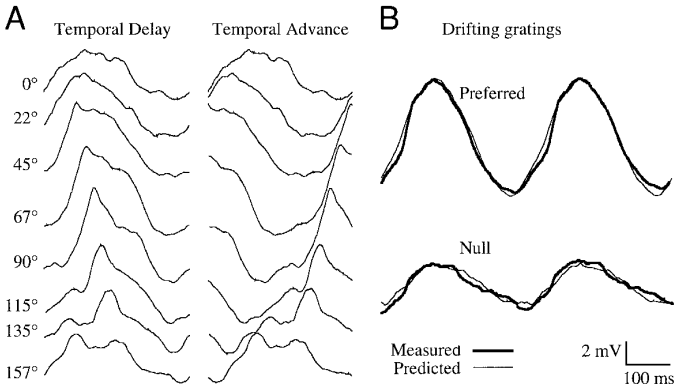

FIG. 6. Application of the data in Fig. 5 to a linear model for the prediction of direction selectivity. *A*: averaged responses to stationary gratings shifted in temporal phase by an amount equal to the spatial phase of the corresponding stimulus. *Left column*: each successive trace has been shifted to the right (temporal delays) to simulate motion to the right. *Right column*: each trace has been shifted to the left (temporal advance) to simulate motion to the left. *B*: thin traces are the sums of the 2 columns in *A* reduced in size by a factor of 4 (see APPENDIX A*1*) and are the predictions of the linear model for the response of the cell to gratings drifting in the 2 directions of motion. Thick traces show the actual response of the cell to the drifting gratings (taken from Fig. 5*B*).

the peaks in time so that each peak is nearly simultaneous with the trough of the response to the stimulus 90° away in spatial phase. As a result, the sums of the traces in the two columns differ in size (Fig. 6*B*, thin traces). The resulting direction selectivity predicted by the model (direction index = 0.47) is close to the direction selectivity exhibited in the cell's actual responses to drifting gratings (direction index = 0.40). Not only is the direction selectivity of the cell predicted correctly, however. The absolute size and shape of the modeled responses closely match those of the cell, including the saw-tooth shape of the nonpreferred response.

The model also correctly predicted the direction selectivity of this simple cell at temporal frequencies other than the optimal. At 1 Hz (Fig. 7) and 4 Hz (not shown), the peak-to-peak amplitude of the response elicited by a grating drifting in the preferred direction of motion was slightly smaller than the amplitude of the response at 2 Hz. In addition, the

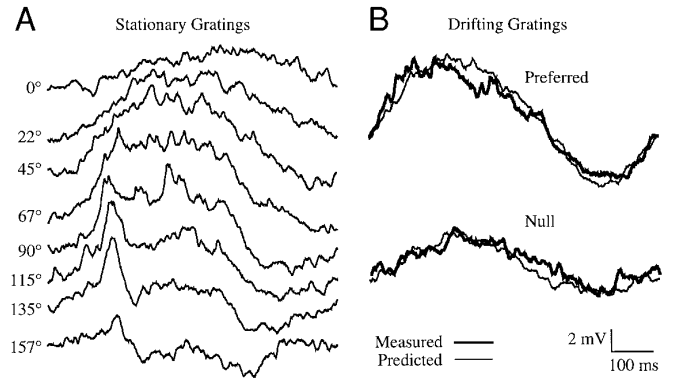

FIG. 7. Linear model applied to the responses of the cell in Fig. 5 to gratings of 1-Hz temporal frequency. *A*: response to contrast reversing gratings of 8 different spatial phases. *B*: response to drifting gratings (thick traces) together with the prediction of the linear model (thin traces) derived from the response to stationary gratings shown in *A*. Only 1 cycle of each averaged response is shown.

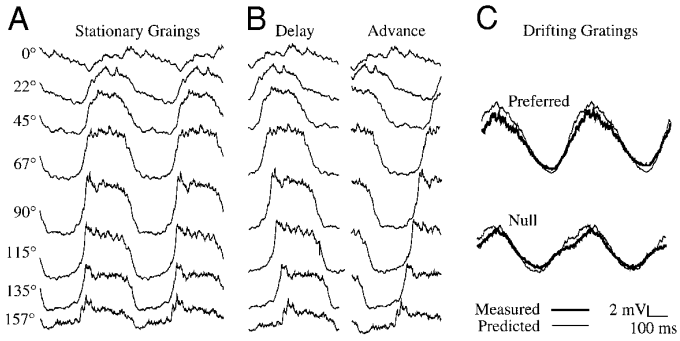

FIG. 8. Third simple cell with moderate direction selectivity. *A*: averaged responses to 2-Hz stationary gratings. *B*: responses of *A* displaced in temporal phase by an amount equal to the spatial phase of the corresponding stimulus. *Left column*: each successive trace has been delayed in time to simulate motion in the preferred direction. *Right column*: each trace has been advanced in time to simulate motion in the nonpreferred direction. *C*: averaged responses to 2-Hz drifting gratings (thick traces), together with the prediction of the linear model of the responses to drifting gratings (thin traces).

response to a grating drifting in the nonpreferred direction was larger than it was at 2 Hz, making the cell significantly less direction selective at these nonoptimal temporal frequencies. The preferred direction of motion was still rightward, however. The responses to stationary gratings at 1 and 4 Hz, like those at 2 Hz, exhibit a shift in temporal phase with stimulus spatial phase. At 1 Hz the shift is over 300 ms between 0 and 135° (Fig. 7*A*); at 4 Hz, the shift is $<$100 ms (not shown). But at each temporal frequency, when the responses to stationary gratings are applied to the linear model, the observed shifts in temporal phase are sufficient to account for the direction selectivity of the cell at that temporal frequency. The resulting predictions for the response to drifting gratings accurately mimic the real responses to drifting gratings (Fig. 7*B*). The direction indices recorded at 1, 2 and 4 Hz were 0.30, 0.40 and 0.26. The modeled direction indexes were 0.36, 0.47, and 0.29.

The polar plot of the temporal phase against response amplitude is shown at 2 Hz for this cell in Fig. 3*I* and for three other cells in Fig. 3, *J*–*L* (*J* is taken from the cell illustrated in Figs. 8 and 12*A*). Each shows a strongly elliptical form (the smooth curves are the closest fitting ellipse) with the ratio of the major and minor axes conforming closely to the cell's direction index. None of these graphs, which are based on intracellular responses, shows the ''wasp waisting'' that is evident in plots made from extracellular responses. The wasp waisting may indeed be the influence of the spike threshold, as suggested by Reid et al. (1987, 1991) and by Tolhurst and Dean (1991). Responses with amplitudes below threshold evoke no spikes, and even above threshold, because of the nonlinear relationship between membrane potential and spike frequency, smaller synaptic potentials evoke disproportionately small numbers of spikes.

Second directional simple cell

The cell illustrated in Fig. 8 was slightly less direction selective than that shown in Fig. 5. Nevertheless, its responses to drifting gratings (Fig. 8*C*) and stationary gratings (Fig. 8*A*) show a similar pattern: the responses to drifting

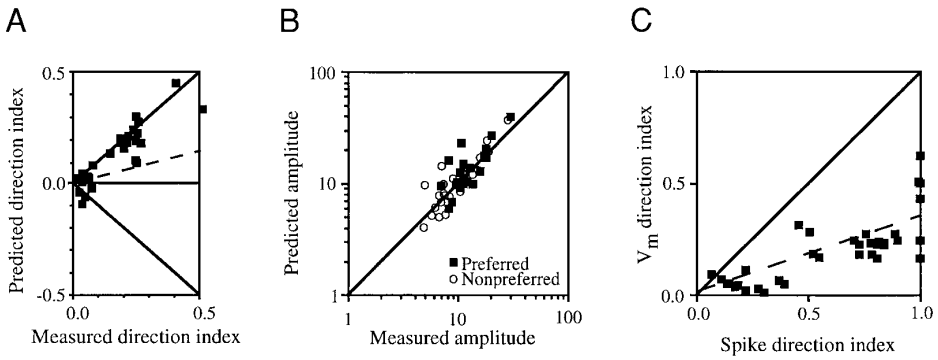

FIG. 9. *A*: linear model's predictions of direction index plotted against the actual direction index for the 14 cells in the sample. More than 14 points are plotted since several neurons were tested at different spatial and temporal frequencies. Points below the *x*-axis indicate that the model predicted the opposite preferred direction from the one actually measured at the same temporal and spatial frequency. Solid line has a slope of 1. Dotted line shows the median ratio between predicted and measured direction indexes derived from extracellular studies of Reid et al. (1991). *B*: amplitude of the response to drifting gratings predicted by the linear model plotted against the actual amplitude of the response to the grating. Filled symbols: preferred direction of motion; open symbols: nonpreferred direction of motion. *C*: direction index derived from fluctuations in membrane potential evoked by drifting gratings, plotted against the direction index derived from intracellularly recorded action potentials taken from the same sets of intracellular records. Solid line has a slope of 1. Dotted line is a linear regression through the points that have not been constrained to cross the origin.

gratings are slightly saw-toothed in shape, and the responses to stationary gratings change shape with changes in stimulus spatial phase. At 0° spatial phase, the cell's response was rounded with a slow rise to the peak; at higher spatial phases, the peak occurred earlier in time. The results of applying the linear model to predict the cell's direction selectivity is shown in Fig. 8, *B* and *C*. In the *left column* of *B*, the responses to the stationary gratings have been shifted in time in the direction appropriate for predicting the preferred (leftward) direction of motion. In the *right column*, the responses have been shifted in the direction appropriate for predicting the nonpreferred (rightward) direction of motion. As for the cell in Fig. 5, the depolarizing phases of the eight traces overlap more closely in time in the *left column* than they do in the *right column*. Because of this difference, the predicted response to the leftward direction of motion is larger than the predicted response to the rightward direction of motion (Fig. 8*C*). The model accurately predicts the direction selectivity of the cell, and the overall shape of the responses to drifting gratings.

Predicted and measured direction index

For the three cells discussed so far, the direction index predicted by the linear model closely matched the direction index measured from the intracellularly recorded responses to drifting gratings. The same was largely true for all 14 cells in the sample. The direction index predicted by the model for each cell is plotted against the measured direction index in Fig. 9*A*. The graph contains more than 14 points because some cells were tested at more than one temporal or spatial frequency. A few of the points in the graph lie below the *x*-axis because the predicted direction index is negative whenever the model incorrectly predicts the preferred direction (see METHODS). Most of the points, particularly those indexes significantly different from zero, lie above the *x*-axis showing that the linear model accurately predicted the preferred direction of the cell in almost all cases, as has been shown in previous extracellular results (Albrecht and Geisler 1991; McLean et al. 1994; Reid et al. 1987, 1991; Tolhurst and Dean 1991). In addition, most of the points lie near the line of slope 1, showing that the model's prediction of direction selectivity closely matched the actual direction selectivity in most cases. The least-squares fit to the data in Fig. 9*A* (not constrained to intercept the origin) has a slope of 0.95, a *y*-intercept of −0.01 and $r = 0.89$.

Predicted and measured amplitudes

Reid et al. (1991) found that a linear model of direction selectivity consistently underestimated the direction selectivity of the cells on average by a factor of 3. The primary reason for the mismatch between the model and the cell's responses to moving gratings was that the model overestimated the response to motion in the nonpreferred direction (Reid 1991, Fig. 9). This was not the case for our intracellular data. The model was equally accurate in its prediction of the amplitude of the response to gratings drifting in both the preferred and nonpreferred direction of motion. This is shown in Fig. 9*B*, where the amplitude of the predicted responses to a drifting grating is plotted against the amplitude of the measured responses for the preferred (filled squares) and nonpreferred (open circles) directions. Overall, there was a slight tendency for the model to overestimate the amplitude of the response (see DISCUSSION), but this trend affected the preferred and nonpreferred responses equally.

Direction index of spike activity

One surprising characteristic of the sample of 14 cells is their seemingly low average direction selectivity. The highest direction index when calculated from fluctuations in membrane potential was 0.51. This is a general feature of intracellular recordings from all classes of cortical cells: in a larger population of 70 neurons, with both simple and complex receptive fields and recorded with both conven-

tional sharp electrodes (Ferster 1986) and patch recording, the maximum direction indexes measured from the membrane potential changes evoked by moving bars or gratings ranged only from 0 to 0.6, with by far the majority falling between 0 and 0.4. In contrast, when direction selectivity is measured extracellularly in a large sample of cells, direction indexes as high as 1.0 are regularly observed (Reid et al. 1991).

The low overall direction selectivity of the fluctuations in membrane potential is not merely the result of a sampling bias of the intracellular electrode. The low direction selectivity seems to stem from a real difference in the amplitude of the direction index calculated from fluctuations in membrane potential and calculated from spike rates. For a given cell and stimulus, the direction index based on fluctuations in V_m is consistently lower than that based on spike rate. This is apparent in Fig. 9*C*, where the two measures are plotted against each other for 26 simple cells in which both measurements were available. For each point, the two different indexes were taken from the same sets of intracellular records, one based on the F1 component of intracellularly recorded spike rates, the other based on the F1 component of membrane potential fluctuations. Those cells in which the spike-generating mechanism was damaged by penetration and in which the number of spikes were consequently few were necessarily excluded. Nevertheless, in those cases where both indexes could be measured, the spike-based direction index was on average 2.9 times greater than the direction index calculated from the intracellular membrane potential. The direction selectivity of the intracellularly recorded sample of cells was therefore not abnormally low. The simplest explanation for the amplification of direction selectivity that occurs at the output stage of simple cells is an expansive nonlinear relationship between membrane potential and spike rate such as would be generated by the spike threshold (Albrecht and Geisler 1991; Heeger 1992). This prediction is borne out in preliminary work. In most of our cells, instantaneous firing rates, and therefore direction indexes, can be predicted accurately by applying a low-pass filter, a threshold, and a linear operator to the membrane potential.

Nature of the synaptic inputs underlying direction selectivity

Although the result of the forgoing analysis is consistent with simple cells summing their inputs linearly, it is by no means proof that they do so. In reconstructing only two responses (those to drifting gratings) from a sum of 8 (those to stationary gratings), some types of nonlinearities could be averaged out and fail to be detected (see APPENDIX C). A much more stringent test of linearity, based on principal component analysis of the eight responses to stationary gratings, was recently developed by one of us (Kontsevich 1995). This analysis showed that the responses of a direction-selective cell can be modeled accurately by a linear combination of only two different sets of synaptic inputs, each with a different time course and receptive-field position. The reconstruction of eight responses from only two principal components is a much more highly constrained test of linearity, similar to solving eight equations with two unknowns. In addition to providing a stringent test of linearity (see APPENDIX C), the analysis revealed some of the characteristics of the input signals: that they were highly linear in spatial summation, that they were linearly related to stimulus contrast, and that they were temporally nonlinear.

The original analysis described was applied by Kontsevich (1995) to the responses of only one direction-selective neuron. The same analysis applied to a more extensive set of simple cells (4 direction selective and one direction insensitive) gave similar results, namely that only two different sets of inputs are required to explain the spatiotemporal inseparability of the receptive fields. From the more extensive set of cells, it can also be seen that the two underlying sets of inputs in each cell are arranged in approximate spatial quadrature, in agreement with the energy models of direction selectivity proposed by Adelson and Bergen (1985) and by Watson and Ahumada (1985).

The method begins with a principal component analysis (singular value decomposition or SVD) of the eight responses to stationary gratings. The SVD generates eight new functions or principal components such that the original responses can be completely reconstructed from linear combinations of these components. But the components are unique in that as much of the signal variance as possible is contained in the fewest number of components. In each of the five cells tested, only the first two principal components contribute significantly to the reconstruction of the data. Fully 98% of the variance of the eight responses can be reconstructed by linear combinations of these two components. (See *Eq.* B*1* in APPENDIX B for the method of measuring the %variance of the data accounted for by the various models.) Surprisingly, the amount of each of the two components present in each of the eight traces varied nearly sinusoidally with the spatial phase of the stationary grating.

This result suggests the parsimonious model in which direction-selective simple cells receive synaptic input from two distinct sets of presynaptic neurons, each one corresponding to one of the two significant principal components, which we will refer to as a subunit. To conform to the results of the SVD, each set of neurons comprising one subunit must be spatiotemporally separable in that their summed responses vary only in amplitude and not in time course with the spatial phase of the stimulus. Second, the underlying neurons must be linear in spatial summation: because the contribution of each principal component to the grating responses varied sinusoidally with spatial phase, then the response of the neurons comprising a subunit can be modeled as varying approximately sinusoidally with stimulus spatial phase. Third, the two subunits must differ from each other in both the spatial position of their receptive fields and in the time course of their responses to the stationary gratings. And finally, the simple cell sums the synaptic inputs from the subunits in a linear fashion. This model can be succinctly stated in the following equation

$$R_\varphi(t) = \sin(\varphi - \chi_1) \cdot P_1(t) + \sin(\varphi - \chi_2) \cdot P_2(t) \qquad (3)$$

Here, φ is the spatial phase of the sinusoidal stimulus, and χ_1 and χ_2 are the spatial phases at which the contribution of each principal component to the reconstructed data falls to zero. P_1 and P_2 describe the temporal waveforms of the two significant principal components. R_φ are not the actual responses of the cell to the eight stationary gratings, but the

TABLE 1. *Results of quasilinear analysis of the responses of four directional and one nondirectional simple cell to stationary gratings*

	Cell			
	1	*2*	*3*	*4*
Figure	11	12*A*	12*B*	12*C*
%Variance in 1st harmonic	92.7	89.6	89.4	90.5
%Variance in higher harmonics	7.3	10.4	10.5	9.5
%Variance overall missed by linear model ($0° < \varphi < 360°$)	3.8	6.1	6.6	5.1
%Variance in odd harmonics	97.2	95.5	94.7	96.1
%Variance in even harmonics	2.8	4.5	5.3	3.9
%Variance of even harmonics missed by quasilinear model	0.3	0.8	0.8	0.8
%Variance of odd harmonics missed by quasilinear model	1.0	1.7	1.4	1.2
%Variance overall missed by quasilinear model	1.3	2.4	2.1	2.0
Ratio of subunit amplitudes (fast/slow)	1.5	1.6	0.9	1.6
Direction selectivity (measured from V_m)	0.41	0.51	0.21	0.15
Relative spatial phases of the subunits	76°	58°	49°	76°
Relative temporal phases of the subunits' 1st harmonics	54°	68°	32°	67°

model's prediction of those responses. As shown in Table 1, with properly chosen variables, *Eq. 3* can account for between 93.4 and 96.2% of the variance of the responses of the four direction-selective cells that were analyzed.

Unfortunately, in a strictly linear model of this nature, neither the relative placement of the receptive fields of the two underlying subunits (χ_1 and χ_2) nor the exact time courses of their responses (P_1 and P_2) can be determined uniquely. Because of the sinusoidal relationship between the responses of the two subunits, and because the sum of two sinusoids is another sinusoid, there are an infinite number of choices for χ_1 and χ_2, and an infinite number of corresponding wave forms for the subunit responses, P_1 and P_2, each of which results in an equally good fit to the data. And although each of the infinite pairs of waveforms are related in that they are linear combinations of one another, the linear model alone cannot be used to determine which of these infinite combinations is correct.

The oversimplifying assumption of the purely linear model (*Eq. 3*) is the key both to finding the exact positions and waveforms of the two inputs, and to improving the fit between the model and the data. This key lies in the model's assumption that a 180° shift in the spatial phase of the stimulus results in an inversion of the responses of the two subunits: because $\sin(x + 180) = -\sin(x)$, this assumption is implicit in the purely sinusoidal relationship in *Eq. 3*. Although the linear model assumes that the entire response of each input varies sinusoidally with the position of the grating stimulus, the responses invariably contain even harmonics, the amplitude of which vary not as the sine of the stimulus position, but as the absolute value of the sine. Thus the even harmonics do not invert when the grating is shifted spatially by 180°. A more complete model of the data that takes the behavior of the even harmonics into account assumes that

$$R_\varphi^{\text{even}}(t) = |\sin(\varphi - \chi_1)| \cdot P_1^{\text{even}}(t) + |\sin(\varphi - \chi_2)| \cdot P_2^{\text{even}}(t) \quad (4)$$

and

$$R_\varphi^{\text{odd}}(t) = \sin(\varphi - \chi_1) \cdot P_1^{\text{odd}}(t) + \sin(\varphi - \chi_2) \cdot P_2^{\text{odd}}(t) \quad (5)$$

where R_φ^{even} and R_φ^{odd} are the summed even and odd harmonics of the model's prediction of the intracellularly recorded responses, P_1^{even} and P_2^{even} are the even harmonics and P_1^{odd} and P_2^{odd} the odd harmonics of the two subunits' responses, and χ_1 and χ_2 are again the spatial phases of the null points of the subunits. Unlike two sine functions, the absolute values of two sine functions do not sum to a third absolute value of a sine. So unlike *Eqs. 3* and *5*, the best fit obtainable between R_φ^{even} in *Eq. 4* and the even harmonics in the data depends critically on the choice of χ_1 and χ_2. This behavior is illustrated in Fig. 10. The even harmonics of the eight traces of Fig. 5*D* are shown in yellow (Fig. 10*A*). Although the even harmonics make up 2.8% of the variance of the traces, because of their narrow peaks and troughs, their amplitudes are as large as 20% of the amplitude of the overall waveform. To obtain the best fit possible from *Eq. 4*, 2,500 evenly spaced combinations of χ_1 and χ_2 were chosen, and the waveforms for P_1^{even} and P_2^{even} that gave the closest fit to the data were derived in each case. The fit (%error) between the resulting R_φ^{even} and the real data was then calculated from *Eq.* B*1* for each of the 2,500 combinations of χ_1 and χ_2 and are plotted in Fig. 10*C*. This graph contains a unique, well-defined minimum for $\chi_1 = -3°$ and $\chi_2 = 73°$ of spatial phase (and for mirror images of this combination). The resulting prediction for the even harmonics of the data, R_φ^{even}, are shown in green superimposed on the yellow data traces in Fig. 10*A*. The corresponding waveforms derived for the even harmonics of the two subunits, P_1^{even} and P_2^{even} are shown in Fig. 10*B*. As calculated from *Eq.* B*1*, the eight R_φ^{even} account for 87% of the variance of the even harmonics of the traces and result in a fit that accounts for all the obvious features of the waveforms. The remaining variance, as can be seen by comparing the yellow and green traces, appears to be largely confined to noise. The well-defined minimum in Fig. 10*C* and the fit between the data and *Eq. 4* give strong confirmation of the result of the principal component analysis, namely that two separable sets of inputs that are summed by the simple cell can account for most of the details of the data.

Once χ_1 and χ_2 are known, it is possible to apply them to a reconstruction of the complete data set. The odd harmonics of the responses are assumed to have the same null points as the even harmonics. The best fitting P_1^{odd} and P_2^{odd} may then be calculated from *Eq. 5*. R_φ, P_1, and P_2 are simply the sums of their even and odd harmonics. These are all shown in Fig. 11, *C* and *D*. The original data and R are superimposed in *C*. The responses of the two subunits are shown in *D*. The two subunits as shown correspond their maximum contributions to the traces in *C*. For example, the maximum response of the first subunit (thick trace in Fig. 11*D*) occurs near 90° spatial phase, and the maximum response of the second subunit (thin trace) occurs near 0°. We refer to *Eqs. 4* and *5* together as a quasilinear model in that synaptic inputs are still summed linearly, but the inputs themselves are no longer perfectly linear in spatial summation. The overall variance accounted for by the quasilinear model improves to 98.7%, compared with the 94.2% accounted for by the purely linear model of *Eq. 3*.

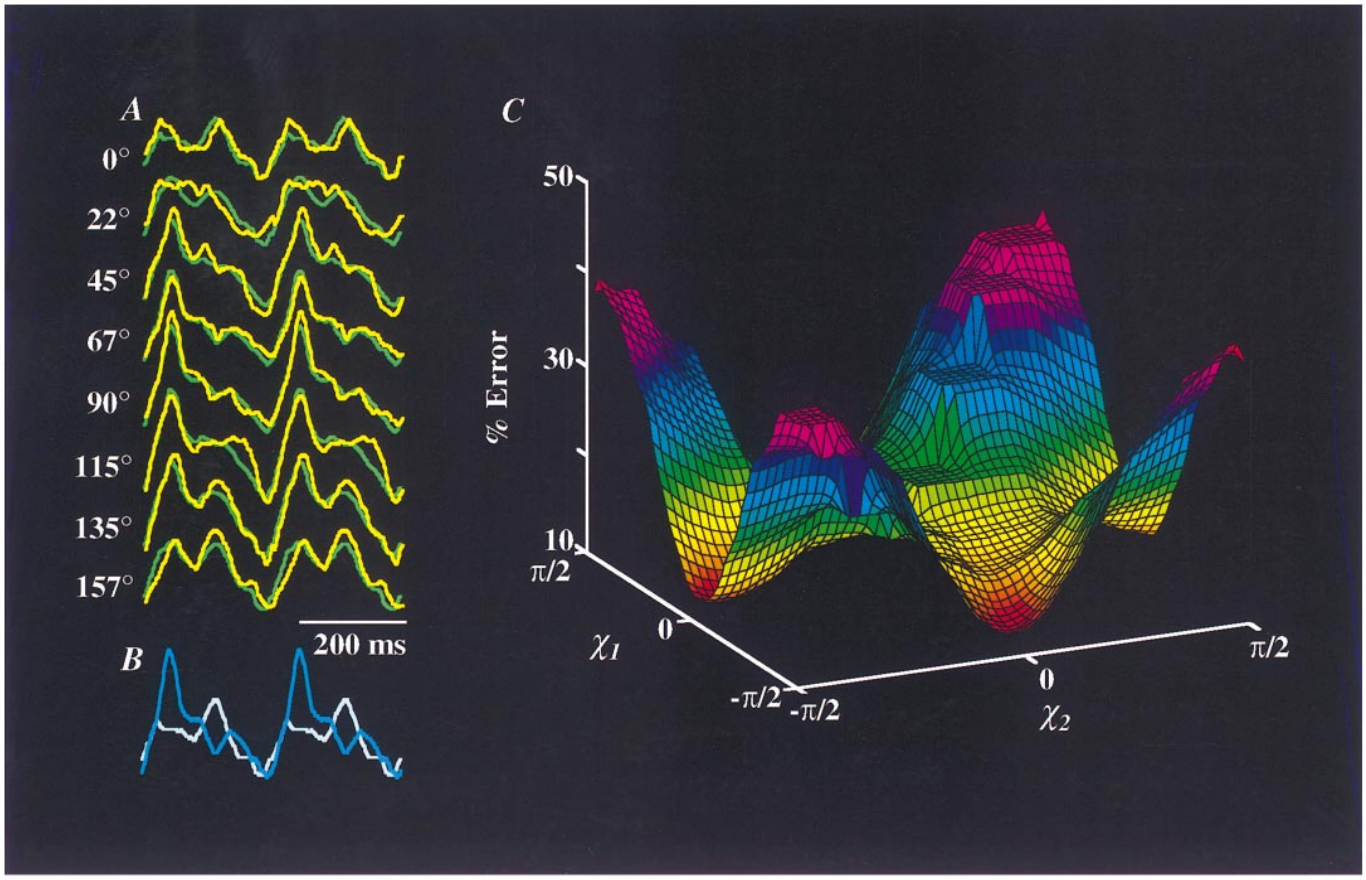

FIG. 10. Two-component quasilinear fit to the even harmonics of the traces shown in Fig. 5*D*. *A*: even harmonics of the traces in Fig. 5*D* (yellow), superimposed on the best fit derived from *Eq. 4* (green traces). Best fit was obtained when χ^1 and χ^2 were set to −3 and 73°. Note that the traces represent 1 cycle of the stimulus (500 ms). *B*: temporal waveforms (P_1^{even} and P_2^{even}) of the 2 components used to construct the green traces in *A*. *C*: %variance of the even components of the intracellular data (R_φ^{even}) not accounted for by *Eq. 4*, plotted against χ^1 and χ^2. Colors are related to the variance at each point and help to make the 3-dimensional shape of the plot easier to interpret. A clear minimum is visible for a pair of values of χ^1 and χ^2 (−3 and 73°) and for their mirror images.

In addition to the responses to 2-Hz stationary gratings shown in Fig. 5*D*, this cell was stimulated with gratings at 1 Hz (Fig. 7) and 4 Hz. When the quasilinear analysis of the underlying subunits was applied to these responses (Fig. 11, *A* and *B*, *E* and *F*), two subunits were again sufficient to account for over 98% of the variance of the traces. And as before, the fit to the even harmonics of the traces yielded a unique combination of receptive-field positions for the subunits (χ_1 and χ_2). The relative displacement between the derived subunits was 58° of spatial phase for the 1-Hz data, and 76° for the 4-Hz data, both in good agreement with the 76° derived from the 2-Hz data, even though they are completely independent measures.

Altogether, the responses of four direction-selective cells to stationary gratings were analyzed by the quasilinear model. The results of the analyses are summarized for the four cells in Table 1. The three additional direction-selective cells and one nondirectional cell are illustrated in Fig. 12. The cell in Fig. 12, *C* and *D*, for example, had a direction index near 0.5. The time-to-peak of the two inputs are so different that, in those traces where both components are present, a small notch is visible between the decay of the first component and the rise of the second (Fig. 12*C*, 67° trace). The quasilinear model is successful in reproducing this feature and overall captures 97.6% of the variance of the traces. The separation between the null points of the subunits is 58°. In the two other direction-selective cells of Fig. 12 (*A* and *B*, *E* and *F*), the model accounts for 97.9 and 98% of the variance in the traces, and the separation of the subunits is 49 and 76°. Finally, the quasilinear analysis of a nondirectional cell (originally illustrated in Fig. 3 of Jagadeesh et al. 1993) is shown in Fig. 12, *G* and *H*. Here again, two subunits are sufficient to account for over 99% of the variance in the data, but the relative contribution of the first component, as indicated in Fig. 12*H*, is overwhelming, so that the eight responses are essentially scaled versions of one another, making the receptive field almost completely spatio-temporally separable.

DISCUSSION

Neurons are complex devices with numerous nonlinear elements including voltage-dependent currents and facilitating synaptic potentials such as those generated by *N*-methyl-D-aspartate (NMDA) receptors. These nonlinear elements are distributed throughout the dendritic tree, the electrical properties of which may further complicate interactions

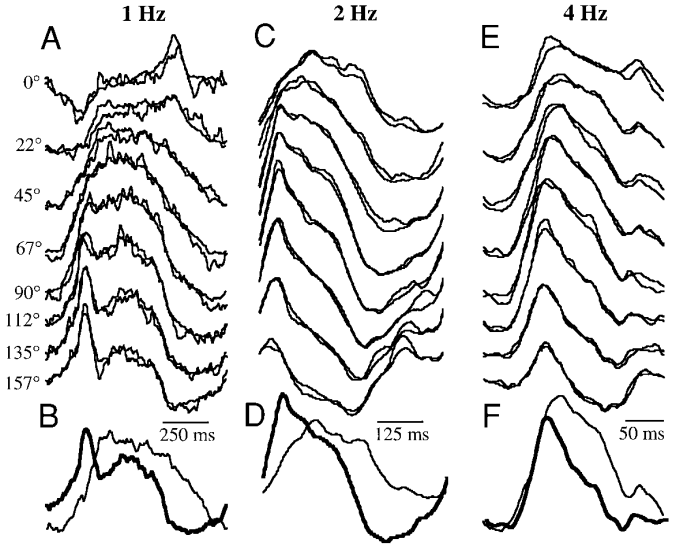

FIG. 11. Quasilinear model applied to the responses of the cell in Fig. 5 to stationary gratings of 3 different temporal frequencies. In the *top panel* of each column (*A, C,* and *E*), the 8 responses are superimposed on the model's predictions of those responses. In the *bottom panel* (*B, D,* and *F*), the waveforms of the 2 subunits are shown. The amplitude of each subunit was chosen to match that subunit's maximal contribution to the reconstructed responses above.

among the different elements. Nevertheless, at least one subset of neurons in the visual cortex behave in a remarkably linear fashion. This result is surprising when one considers the special relationship among synapses located near one another in the dendritic tree: an active synapse could influence the potentials generated by other nearby synapses in at least two ways. First, the membrane conductance of an active synapse could cause a large, local reduction in the input resistance of the dendrite. Second, the depolarization caused by the first active synapse could reduce the driving force on the synaptic currents generated at other subsequently activated synapses. Both of these mechanisms imply that an active synapse will reduce the size of synaptic potentials arising from nearby active synapses relative to the potentials they would produce when activated alone (Koch et al. 1990).

Nevertheless, under the conditions of our experiment, these types of nonlinear interactions among nearby synapses do not appear. It is possible that the success of the linear prediction of direction selectivity might have missed some nonlinear processes since eight responses to stationary gratings were combined to generate the two responses to moving gratings. In theory, some nonlinearities might have been averaged out in the process. The quasilinear analysis of Figs. 10–12 is a much more stringent test of linearity, however, in that all eight responses to the stationary gratings are reconstructed from only two subunit responses. A linear system of eight equations in only two unknowns is sufficient to characterize the eight independent responses. These results suggest that nonlinear interactions among nearby synapses either are insignificant in these cells, or that nearby synapses are rarely activated simultaneously. Alternatively, nonlinear interactions among nearby synapses might occur, but be compensated for by amplifying processes in the dendrites, such as NMDA-mediated potentials or voltage-dependent Na^+ and Ca^{2+} currents similar to those reported by Stuart and Sakmann (1994) in neocortical pyramidal cells. It is interesting in this regard that iontophoretically induced ''synaptic'' potentials in cultured pyramidal cells also sum in a highly linear fashion (Cash and Yuste 1997). Alternatively, linearity might emerge as a network property of the cortical circuit as a whole (Douglas et al. 1995). The question then arises as to why cortical neurons go to such lengths to linearize local synaptic interactions and what the computational significance of this might be. It should be stressed, however, that the cells conform to a linear model only for the averaged responses to one limited set of stimuli and for one subset of neurons in the visual cortex, the simple cells in layers 3 and 4. Significant nonlinearities might emerge under other experimental circumstances.

Poggio and Reichardt's (1973) proof that motion detection requires some form of nonlinearity would seem to contradict the suggestion that direction selectivity of synaptic potentials arises solely from linear summation mechanisms. Movshon et

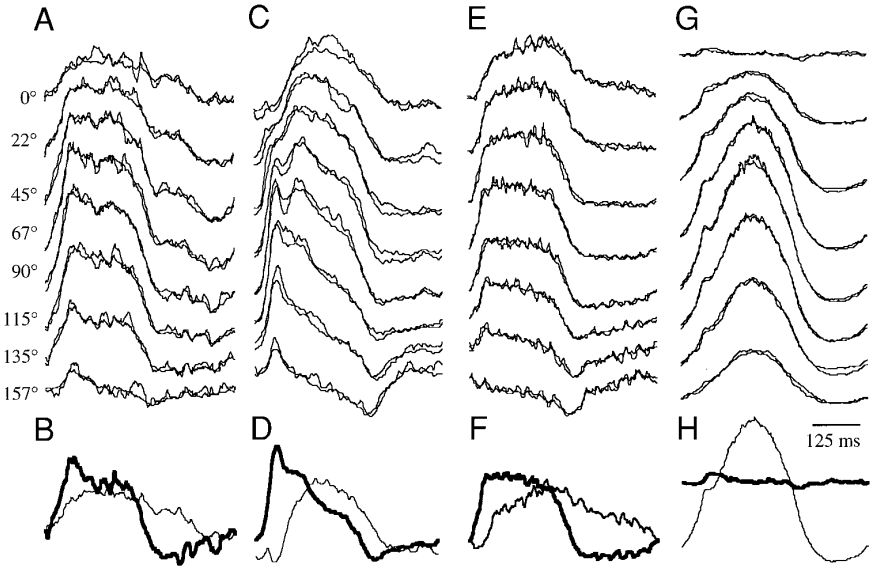

FIG. 12. Quasilinear model applied to the responses of 4 cells, 3 of which were direction selective (*A–E*) and 1 of which was nondirectional (*G* and *H*). In the *top panel* of each column (*A, C, E,* and *G*), the 8 responses are superimposed on the model's predictions of those responses. In the *bottom panel* (*B, D, F,* and *H*), the waveforms of the 2 subunits are shown. The amplitude of each subunit was chosen to match that subunit's maximal contribution to the reconstructed responses above.

al. (1978), however, point out that nonlinearity is required only to produce differences in the mean levels of response, not the modulations around the mean. Linear summation of two signals in spatiotemporal quadrature can produce 100% direction selectivity of the modulated signal. In our analysis, only the amplitude of the visually evoked oscillation was measured and modeled with linear mechanisms, not any possible changes in the mean level of the membrane potential. Poggio and Reichardt's requirements for nonlinearities therefore do not apply to this case (Reid et al. 1991). Nevertheless, the responses of simple cells when measured extracellularly do show a difference in the mean rate of firing in response to different directions of motion. Preliminary analysis shows little evidence for large dependence of the mean membrane potential on stimulus direction. Therefore, at some stage between the summation of synaptic potentials and the generation of action potentials, there must be a nonlinearity that at least partially underlies the extracellularly detected changes in mean firing rate with direction.

The extracellular data when considered alone left open a number of possibilities for the source of this nonlinearity. Dean et al. (1980) proposed a shunting inhibition evoked by stimuli of the nonpreferred direction to explain their extracellular data, and other theoretical treatments of direction selectivity have relied on shunting inhibition (Grzywacz and Koch 1987; Koch et al. 1982; Torre and Poggio 1978). But shunting inhibition requires nonlinear summation of synaptic potentials and so seems unlikely given the result presented here. In addition, shunting requires significant visually evoked changes in neuronal input resistance, which have not been found intracellularly (Douglas et al. 1988; Ferster 1986; Ferster and Jagadeesh 1992). This leaves as a likely candidate for the extracellularly observed nonlinearity a nonspecific mechanism such as the spike threshold (Reid et al. 1991). But although threshold is a powerful nonlinearity, a threshold followed by a linear relationship between membrane potential and spike rate is insufficient to account for the extracellular data. An additional nonlinear relationship between membrane potential above threshold and spike rate is needed, such as the half-squaring mechanism of Heeger (1992) or the expansive nonlinearity of Albrecht and Geisler (1991). Using a threshold and an expansive nonlinearity, these latter authors were able to predict the extracellularly measured direction selectivity of cortical neurons from their responses to stationary stimuli. Threshold together with an additional nonlinearity would largely explain the two- to threefold increase in direction selectivity of cells measured from their firing rates compared with the direction selectivity measured from changes in membrane potential (Fig. 9*C*). Thresholds are static nonlinearities, however, and are very different in character from a visually evoked nonlinear shunt, the amplitude of which depends on stimulus direction.

Heeger (1992) and Albrecht and Geisler (1991) have proposed the presence of a third nonlinearity in simple cells, contrast normalization. They demonstrate that the synaptic inputs to simple cells must somehow be scaled down by a signal proportional to the stimulus contrast before they are converted to the output train of action potentials. Without a contrast normalization process, the tuning of simple cells for stimulus properties such as orientation or direction would change with stimulus contrast, in part because of response saturation at high contrasts. Depending on whether contrast normalization occurs before, during, or after the summation of synaptic potentials, it could in theory be detectable in intracellular records like those presented here. In neither case, however, would normalization affect the linear model's prediction of the direction index, because normalization would scale the responses to the preferred and nonpreferred directions of motion equally.

Mechanisms underlying spatiotemporal inseparability in simple cells

The quasilinear analysis embodied in *Eqs. 4* and *5* has a number of properties that make specific predictions about the organization of the synaptic inputs to direction selective simple cells.

1) The receptive fields are made up of at least two functional subunits with different response time courses. On average, the two-subunit model accounted for all but 2% of the variance of the traces, as defined by *Eq.* B*1*. This is an impressively high amount given that the traces inevitably contained some noise. In addition, the smooth surface in Fig. 10*C* has no local minima, which means that the spatial phases of the null points of the subunits could be uniquely and precisely identified, which in turn uniquely specifies the waveforms representing the subunits' responses. A third indication of the significance of the analysis is that independent derivations of the relative positions of the null points for the cell in Fig. 11, using stimuli of three different temporal frequencies, give values in close agreement. Nevertheless, these fits between the data and the model do not demonstrate unequivocally that there are no more than two subunits (see APPENDIX C). Under certain circumstances, the principal component analysis could miss a larger number of distinct subunits, lumping them together into two components.

However many subunits there are, each functional spatiotemporally separable subunit to which we refer is likely made up of synaptic input from many neurons and from a number of different sources, including, geniculate and cortical cells, ON- and OFF-center cells, and excitatory and inhibitory cells. The multiple synaptic inputs of each subunit act as one mechanism for the purpose of our analysis either because their receptive fields are superimposed in space or because they have similar response waveforms. With different stimuli, no doubt more subdivisions of the inputs would emerge. More specific suggestions for the origin of these synaptic inputs are made below.

2) Each subunit is highly linear in spatial summation. The presence of the null points in the responses of the subunits and the sinusoidal dependence of subunit response amplitude on spatial phase require this subunit linearity. It also is likely that the neurons that combine to make up the subunit are linear in spatial summation and therefore either are, or receive input from, X relay cells of the LGN. This latter conclusion derives from the relative lack of second harmonics in the responses to stationary gratings. Overall, the total contribution to each subunit from even harmonics is $<3\%$, and their amplitudes are strongly modulated by the spatial phase of the stimulus. The even harmonics of Y cells' responses, by comparison, are stronger and are invariant with spatial phase (Hochstein and Shapley 1976). The lack of observed Y cell input is consistent with previous extracellular mea-

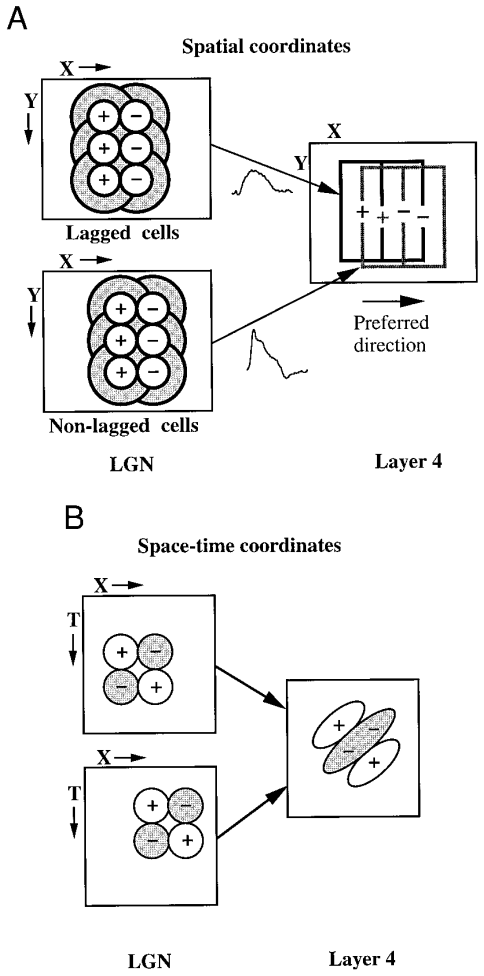

FIG. 13. Schematic diagram of the inputs to a direction-selective simple cell. *A*: the spatial receptive field of the simple cell is depicted as being constructed of inputs from lagged and nonlagged geniculate relay cells. The receptive fields of the lagged and nonlagged inputs are each arranged in rows to generate orientation selectivity in the simple cell according to the scheme proposed by Hubel and Wiesel (1962). The receptive fields of the lagged and nonlagged cells are displaced from one another by $\sim$½ the diameter of a receptive-field center. Together with the temporal delay between the nonlagged and lagged cells, the spatial offset of the 2 cell types generates direction selectivity in the postsynaptic simple cell. All inputs are depicted as monosynaptic, but the input from either the lagged or nonlagged cells or both could be relayed to the simple cell by an excitatory or inhibitory cortical interneuron, which would itself have a nondirectional simple receptive field. *B*: receptive fields of the lagged and nonlagged inputs and of the direction-selective simple cell plotted in space-time coordinates.

surements of spatial linearity of neurons in area 17 (Ferster and Jagadeesh 1991; Spitzer and Hochstein 1985).

3) The subunit responses are temporally nonlinear, as defined by the presence of higher harmonics of the stimulus temporal frequency in the subunit responses. This nonlinearity no doubt arises from the temporal nonlinearities of responses of presynaptic geniculate relay cells, and of other cortical neurons. Cortical neurons in particular have temporally nonlinear responses because of their lack of spontaneous activity and the resulting half-wave rectification.

Motion detection models

One striking outcome of the analysis of direction selectivity presented here is how closely the resulting picture of the visual system resembles the energy models of motion detection proposed by Adelson and Bergen (1985) and by Watson and Ahumada (1985). These models consist of four separate stages. The first stage consists of two spatiotemporally separable linear filters with their spatial positions and temporal responses offset from one another (Fig. 13*B, left*). These are combined linearly to produce the second stage, a spatiotemporally inseparable direction-selective filter (Fig. 13*B, right*). In the third stage, the output of two spatiotemporally oriented filters with similar preferred direction and offset spatial position are individually squared and summed to give a time-invariant output, which is proportional to motion energy. Finally, two direction energy units with opposite preferred directions are differenced to generate a single motion opponent signal, which is positive for a stimulus of the preferred direction and negative for a stimulus of the nonpreferred direction.

According to the quasilinear analysis, directional simple cells are nearly identical to the second stage of the energy model, whereas the underlying subunits resemble the first stage. There are several points of similarity between the energy models and our model of simple cells. *1*) The direction-selective cells combine only two spatiotemporally separable subunits, the minimum number possible. *2*) The signals from the two subunits are combined in a strictly linear fashion. *3*) The spatial phase shift between the subunits is compatible with the quadrature relation approximating 90° for most of the cells (Table 1). What we do not know is whether the spatial phase relationship between the subunits is invariant with spatial frequency; as it is in the energy models. In practice, designing a neuronal mechanism with this property is difficult. More likely, the phase relationship changes for stimulus spatial frequencies away from the peak. If so, since the spatial frequencies tested in the search of the optimum differed by a factor of $\sqrt{2}$ there might have been a spatial frequency at which the subunits were more nearly in spatial quadrature. *4*) A final prediction of the energy model is that the subunits are separated by 90° in temporal phase. The temporal phase differences observed between the two subunits for the four cells analyzed ranged from 32 to 68° at the fundamental stimulus frequency (2 Hz). These numbers are significantly less than 90°, but they do not reflect the true temporal differences between the subunit responses because the responses contain significant components at frequencies higher than the fundamental.

Although the properties of simple cells resemble the energy models of motion perception, they are inconsistent with highly nonlinear correlation models in which the responses from different spatial locations are multiplied together after one of the signals is delayed (Reichardt 1961; van Santen and Sperling 1984). Although the final output of a Reichardt model, a single signed value indicating direction of motion, is identical to that of an energy model, the calculations performed at the intermediate stages of the two models are very different from one another (Emerson et al. 1992). The responses of simple cells to a drifting grating resemble none of the responses of the intermediate stages of the Reichardt models as closely as they do the spatiotemporally oriented filters of the energy models. Emerson et al. (1992) have found a corresponding result for cortical complex cells in that their unmodulated direction-selective output resembles

the third stage of the energy models (the motion energy detectors) and are inconsistent with any stage of the Reichardt model.

Origin of temporally delayed inputs

The results presented here do not provide complete information about the spatial organization of the receptive fields of the two subunits (if indeed there are only 2), or about the neuronal substrate of the subunits. From other work, however, it is possible to construct a plausible model for direction selectivity in simple cells. The model is diagrammed in Fig. 13*A* and is based on a proposal from Saul and Humphrey (1992a,b). These authors provide evidence that the short- and long-phase delayed signals underlying direction selectivity originate from lagged and nonlagged relay cells of the LGN. In Fig. 13*A*, then, the subunits giving rise to the two inputs are depicted as being constructed from lagged and nonlagged cells. The presynaptic neurons of each cell type are arranged in rows according to the model of orientation selectivity proposed by Hubel and Wiesel (1962). The receptive fields of the two subunits are displaced from one another by approximately one-half the diameter of the geniculate receptive-field centers, which corresponds to ~90° of spatial phase at their preferred spatial frequency. The presynaptic lagged and nonlagged cells are shown providing input to both the ON and OFF subregions of the simple cell's receptive field. In this way, each subregion becomes direction selective in its own right, in accordance with the arrangement of the receptive fields of some of the neurons illustrated by McLean et al. (1989, 1994).

This model is oversimplified in several aspects. First, the segregation of lagged and nonlagged inputs into the two subunits may not be complete. There might be mixtures of lagged and nonlagged into the subunits, with one or the other predominating. The degree of segregation, could, for example, determine the difference in timing of the subunits, which would in turn affect the degree of direction selectivity of the cell. Second, there could be some overlap in the properties of the neurons that provide input to the two subunits. Finally, the cortical inputs that surely contribute to the responses of the recorded neurons are not included in the model. Among these are the spatially opponent inhibitory inputs that generate ON inhibition in the OFF region, and OFF inhibition in the ON region (Ferster 1988; Heggelund 1986; Hubel and Wiesel 1962; Palmer and Davis 1981). Each subunit could have its own inhibitory inputs of matching type, with the lagged ON subregion receiving OFF inhibition mediated by lagged cells, and the lagged OFF region receiving ON inhibition mediated by lagged cells. Alonso et al. (1995) have provided evidence for spatially and temporally offset inhibition that might contribute to direction selectivity, although the origin of the delays is not known. Douglas et al. (1995) and Maex and Orban (1996) assign even more importance to the intracortical circuitry, suggesting that excitatory cortical feedback loops selectively amplify weak geniculate signals generated by stimuli of the preferred direction. These authors have shown in neural simulations that an intracortical feedback network differs in critical ways from the predominately feed-forward model that we propose, yet the models can still be designed so that responses to drifting gratings can be predicted by responses to stationary gratings.

In the model of Fig. 13*A*, the excitatory lagged and nonlagged cells are both shown synapsing directly onto the simple cell. At least some of the geniculate relay cells must do so, because all the simple cells in our sample received some monosynaptic input from relay cells. It is possible, however, that the input from one set of relay cells, either the lagged or the nonlagged, might be relayed to the simple cell through a second simple cell with a spatiotemporally separable receptive field. Alternatively, it is possible that the delay, which in the model is generated by lagged cells, is instead generated entirely within the cortex. For example, the relay cells that are depicted as lagged, might instead be nonlagged. They could in turn project to a cortical cell with a spatiotemporally separable simple receptive field, which delays the signal and sends it on to the direction-selective cell. An elegant proposal for generating temporal shifts from the use-dependent depression of intracortical synapses has been proposed by Abbott et al. (1996), who were able to model precisely records like those in Fig. 5. There is some experimental evidence for a cortical contribution to or even for a cortical origin of direction selectivity: Sillito (1977) found that bicuculline iontophoresed locally into the cortex reduces direction selectivity, whereas Wolmann and Palmer (1993) found that blockage of GABAergic inhibition in the visual cortex can reduce the spatiotemporal inseparability of simple cells. On the other hand, Ferster et al. (1995) have shown that selectively suppressing activity in the cortical circuit by cooling leaves the directionality of input to simple cells largely intact, suggesting that the thalamic input by itself is strongly directional. The complete explanation of direction selectivity might ultimately include contributions both from cortical and thalamic sources. But whatever the source of the inputs of different time course, it remains one of the major pieces missing from our understanding of the origin of direction selectivity in the cat striate cortex. It will surely be the subject of intense study for some time to come.

APPENDIX A

The luminance profile of a drifting grating of contrast C and spatial and temporal frequencies of ω_{tf} and ω_{sf} is

$$L_{\text{drifting}} = C \cdot \sin\ (\omega_{sf} \cdot x \pm \omega_{tf} \cdot t)$$

The ''+'' and ''−'' represent the two possible directions of motion. The luminance profile of one of the eight stationary, contrast-modulated gratings is

$$L_{\text{stationary}}(n) = C \cdot \sin\left(\omega_{sf}x + n \cdot \frac{\pi}{8}\right) \cdot \sin\ (\omega_{tf}t)$$

for $n = 0$ to 7. Through the application of the trigonometric identity, $\sin\ (x + y) = \sin\ (x) \cdot \cos\ (y) + \cos\ (x) \cdot \sin\ (y)$, it can be shown that the drifting gratings can be expressed as a sum of the eight contrast-modulated gratings if these are shifted appropriately in temporal phase

$$\sum_{n=0}^{7} L_{\text{stationary}}(n) = \sum_{n=0}^{7} C \cdot \sin\left(\omega_{sf}x + n \cdot \frac{\pi}{8}\right) \cdot \sin\left(\omega_{tf}t \pm n \cdot \frac{\pi}{8}\right)$$

$$= C \cdot \cos\ (\omega_{sf}x) \cdot \sin\ (\omega_{tf}t) \cdot \sum_{n=0}^{7} \sin\frac{n\pi}{8} \cdot \cos\frac{n\pi}{8}$$

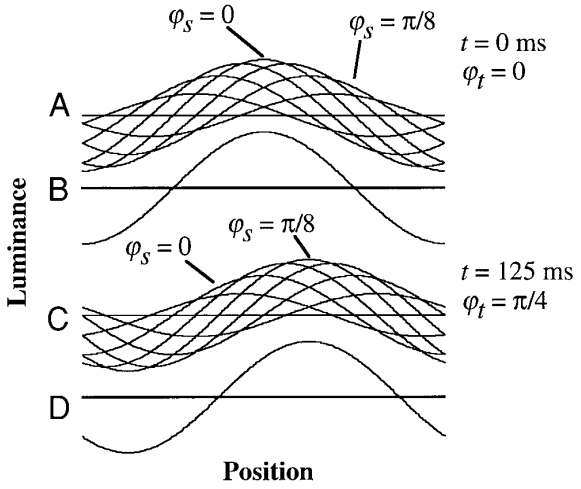

FIG. A1. Sum of a series of stationary contrast reversing sine-wave gratings is a drifting sine-wave grating of the same spatial frequency. *A*: luminance profiles of the 8 stationary gratings frozen at one moment in time. Each grating has a slightly different spatial phase and so a slightly different peak position. Equally important, each grating has a slightly different temporal phase so that the contrast of each grating is slightly different at this moment in time. *B*: the sum of the 8 stationary gratings, scaled by a factor of 1/4. *C*: same 8 stationary gratings as in *A*, but later in time by 1/16th of a temporal cycle. Note that the grating that was at maximum contrast in *A* now has diminished contrast (arrow), while other gratings have increased in contrast. *D*: sum of the 8 component gratings. Although its amplitude has not changed from *B*, its position has shifted to the right.

$$+ C \cdot \sin(\omega_{sf}x) \cdot \sin(\omega_{tf}t) \cdot \sum_{n=0}^{7} \left(\cos\frac{n\pi}{8}\right)^2$$

$$\pm C \cdot \cos(\omega_{sf}x) \cdot \cos(\omega_{tf}t) \cdot \sum_{n=0}^{7} \left(\sin\frac{n\pi}{8}\right)^2$$

$$\pm C \cdot \sin(\omega_{sf}x) \cdot \cos(\omega_{rf}t) \cdot \sum_{n=0}^{7} \sin\frac{n\pi}{8} \cdot \cos\frac{n\pi}{8}$$

But since

$$\sum_{n=0}^{7} \sin\frac{n\pi}{8} \cdot \cos\frac{n\pi}{8} = 0 \quad \text{and} \quad \sum_{n-0}^{7} \left(\cos\frac{n\pi}{8}\right)^2 = \sum_{n=0}^{7} \left(\sin\frac{n\pi}{8}\right)^2 = 4$$

then

$$\sum_{n=0}^{7} L_{\text{stationary}}(n) = 4C \cdot \sin\left(\omega_{sf} \cdot x \mp \omega_{tf} \cdot t \pm \frac{\pi}{2}\right) = 4 \cdot L_{\text{drifting}} \quad \text{(A1)}$$

A graphical representation of this equation is shown in Fig. A1. Figure A1*A* shows the luminance profiles of the eight stationary gratings at $t = 0$. Each grating has a slightly different spatial phase and so a slightly different peak position. Equally important, each grating has a different temporal phase so a different contrast, as well. The sum of the eight stationary gratings, scaled by a factor of one-fourth is shown in Fig. A1*B*. At time $t = \pi/8$, the stationary grating that had maximum contrast in *A* now has diminished in contrast, while other gratings have increased in contrast. The sum of the eight component gratings (Fig. A1*D*) remains a sine wave, with identical amplitude as in *A*, but a different position. The sum of the eight contrast-reversing gratings is therefore a moving grating in one direction, drifting to the right in this case because the temporal phase of each stationary grating was delayed with respect to its neighbor to the left. If the temporal phase of each grating were advanced with respect to its left-hand neighbor, the sum would drift to the left instead.

Combining *Eqs. 1* and A*1*, for a linear cell

$$\mathbf{R}\left[C \cdot \sin\left(\omega_{sf} \cdot x \mp \omega_{tf} \cdot t \pm \frac{\pi}{2}\right)\right]$$

$$= \frac{1}{4}\sum_{n=0}^{7} \mathbf{R}\left[C \cdot \sin\left(\omega_{sf}x + n \cdot \frac{\pi}{8}\right) \cdot \sin\left(\omega_{tf}t \pm n \cdot \frac{\pi}{8}\right)\right]$$

For example, the response of a linear cell to a drifting sine wave grating should equal the sum of the scaled, temporally shifted responses to the stationary gratings.

APPENDIX B

The error in the predictions of the linear and quasilinear models were calculated according to the following equation

$$\%\text{error} = 100 * \frac{\sum_{\varphi=0}^{7}\sum_{t=0}^{\pi}(R_\varphi - D_\varphi)^2}{\sum_{\varphi=0}^{7}\sum_{t=0}^{\pi} D_\varphi^2} \quad \text{(B1)}$$

where D_φ are the eight responses of a cell to stationary gratings at eight different spatial phases, and R_φ are the eight simulations of these responses derived from the singular value decomposition, the purely linear model (*Eq. 3*), or the quasilinear model (*Eqs. 4* and *5*).

APPENDIX C

The cells in our sample appear to be highly linear when tested with the two methods embodied in *Eqs. 1*, *4*, and *5*. The question is how stringent are these tests? How nonlinear could the cells be and still appear linear given the properties of the tests themselves, and given that the data are noisy? To determine the sensitivity of the various methods, we deliberately introduced artificial nonlinearities into the data and measured how well the models detected them. We distorted the various waveforms of the models with the sign-preserving power nonlinearity, $y = \text{sign}(x) \cdot \text{abs}(x)^p$ and asked how far p could be changed from 1 and still have the data conform well to the linear models.

For the quasilinear model of Figs. 10–12, for example, the power nonlinearity was used to distort either the subunit gains or instantaneous outputs (early nonlinearities), or the output of the summation stage (late nonlinearity). These distortions were applied to the responses of the first cell in Table 1, and the resulting responses were processed with the quasilinear analysis scheme of *Eqs. 4* and *5*. We then estimated the range of admissible values for the nonlinearity parameter p as the range for which the resulting discrepancies were less than the error of the quasilinear fit to the real data (i.e., <1.3% of the overall energy). In fact, this procedure somewhat exaggerates the ranges for p because some unknown part of the error is due to noise. Our analysis showed that, for each nonlinearity considered, the range for p was between 0.7 and 1.4. This is quite a narrow range, and it becomes even smaller if several nonlinearities act together.

The next issue that we studied by simulation was the predictability of drifting grating responses by the quasilinear model. The drifting grating response, according to this model, ought to be the sum of the two subunit profiles with the proper temporal delay. Such simulation with the reconstructed subunits provided a reasonable residual error of 5.3%. When we optimized the phases of the subunits (and correspondingly their profiles) to improve the fit, the lowest error value was 4.0%. These fits, although quite tight, had greater errors than the 2.8% error provided by the standard linearity test described in APPENDIX A or the 1.3% fit of the quasilinear model for counterphasing gratings. The small increase in error for the quasilinear prediction occurred because the high-frequency

features of the subunit responses did not cancel each other when we added just two subunit profiles, and the resulting predictions for drifting gratings were lumpier than the recorded profiles. We do not have a clear explanation for the smoothness of the drifting grating responses.

In the next test we estimated the validity of the linearity test with summation of counterphase gratings described in *Eq. 1* and APPENDIX A. As we did to evaluate the precision of the direct quasilinear model, we generated predicted responses to counterphasing gratings for the quasilinear model with nonlinearities at different stages. We now summed up the counterphase responses with temporal delays appropriate for a drifting grating stimulus (as we describe in APPENDIX A) and compared the results with the direct quasilinear model prediction for drifting gratings. We found that the admissible range for p was between 0.5 and 2 for all nonlinearities except the late one, which had even larger range. Thus we conclude that the traditional linearity test is about one-half as sensitive (on a log scale) to the nonlinearities of the intermediate stages as the quasilinear analysis.

The last test was related to the number of the subunits. Kontsevich (1995) mentioned that two-factor, linear, and quasilinear analyses, even if they would provide a perfect fit to the data, could not reveal the number of the subunits if some of the subunits have linear responses. In this series of computational experiments, we studied how additional subunits with realistic nonlinear temporal waveforms affect the precision of the fit. We simulated the outputs of the cells that contained either three or a continuum of subunits. The fastest and the slowest subunits had standard profiles, and the intermediate subunits were obtained by smooth interpolation. Then we applied the two-factor model to the resulting signals and computed how much it accounted for the variance of the higher harmonics (it would be unfair to compare the overall precision because the contribution of the higher harmonics diminishes with the number of subunits). The general result was that the two-factor model accounted for 94.2–94.3% of the higher harmonic variance: much more than 81.6% obtained for the recordings. [Kontsevich (1995) said that the precision of the 2-factor model was 83.8% rather than the 81.6% provided here: this discrepancy arises because that paper utilized scanned data, as opposed to the original data set analyzed here.] Thus the precision of the model fit is insufficient to make a conclusive statement about the number of the subunits. We consider the two-subunit assumption to be the most parsimonious and use it throughout the analysis presented in this paper.

The authors are grateful for comments from E. Adelson, M. Carandini, D. Heeger, C. Koch, C. Reid, and M. Stryker.

This work was supported by National Eye Institute Grant R01-EY-04726 and the McKnight Endowment Fund for Neuroscience.

Address for reprint requests: D. Ferster, Dept. of Neurobiology and Physiology, 2153 North Campus Dr., Northwestern University, Evanston, IL 60208.

Received 11 January 1997; accepted in final form 24 July 1997.

REFERENCES

ABBOTT, L. F., SEN, K., VARELA, J. A., GIBSON, J., AND NELSON, S. B. Functional consequences of synaptic depression for response properties in V1. *Soc. Neurosci. Abstr.* 22: 952, 1996.

ADELSON, E. H. AND BERGEN, J. R. Spatiotemporal energy models for the perception of motion. *J. Opt. Soc. Am.* 2: 284–299, 1985.

ALBRECHT, D. G. AND GEISLER, W. S. Motion selectivity and the contrast-response function of simple cells in the visual cortex. *Vis. Neurosci.* 7: 531–546, 1991.

ALONSO, J. M., HIRSCH, J. A., AND REID, R. C. The intracellular responses produced by moving and static stimuli are well matched in simple cells. *Soc. Neurosci. Abstr.* 21: 21, 1995.

BARLOW, H. B. AND LEVICK, W. R. The mechanism of directionally selective units in the rabbit's retina. *J. Physiol. (Lond.)* 78: 477–504, 1965.

BISHOP, P. O., COOMBS, J. S., AND HENRY, G. H. Receptive fields of simple cells in the cat striate cortex. *J. Physiol. (Lond.)* 231: 31–60, 1973.

BLANTON, M. G., LO TURCO, J. J., AND KRIEGSTEIN, A. R. Whole cell recording from neurons in slices of reptilian and mammalian cerebral cortex. *J. Neurosci. Methods* 30: 203–210, 1989.

BURR, D. C. Temporal summation of moving images in the human visual system. *Proc. R. Soc. Lond. Ser. B* 211: 321–339, 1981.

BURR, D. C., ROSS, J., AND MORRONE, M. C. Seeing objects in motion. *Proc. R. Soc. Ser. B* 227: 249–265, 1986.

CASH, S. AND YUSTE, R. Spatial integration of subthreshold excitatory inputs by cultured hippocampal neurons. *Neurosci. Abstr.* 23: 1129, 1997.

DEAN, A. F., HESS, R. F., AND TOLHURST, D. J. Divisive inhibition involved in direction selectivity (Abstract). *J. Physiol. (Lond.)* 308: 84P–85P, 1980.

DEANGELIS, G. C., OHZAWA, I., AND FREEMAN, R. D. Spatiotemporal organization of simple-cell receptive fields in the cat's striate cortex. II. Linearity of temporal and spatial summation. *J. Neurophysiol.* 69: 1118–1135, 1993.

DOUGLAS, R. J., KOCH, C., MAHOWALD, M., MARTIN, K.A.C., AND SUAREZ, H. H. Recurrent excitation in neocortical circuits. *Science* 269: 981–985, 1995.

DOUGLAS, R. J., MARTIN, K.A.C., AND WHITTERIDGE, D. Selective responses of visual cortical cells do not depend on shunting inhibition. *Nature* 332: 642–644, 1988.

EMERSON, R. C., BERGEN, J. R., AND ADELSON, E. H. Directionally selective complex cells and the computation of motion energy in cat visual cortex. *Vision Res.* 32: 203–218, 1992.

EMERSON, R. C. AND CITRON, M. C. Linear and nonlinear mechanisms of motion selectivity in simple cells of the cat's striate cortex. In: *Nonlinear Vision: Determination of Neural Receptive Fields. Function and Networks.* Boca Raton, FL: CRC, 1992, p. 75–89.

EMERSON, R. C. AND GERSTEIN, G. L. Simple striate neurons in the cat. II. Mechanisms underlying directional asymmetry and direction selectivity. *J. Neurophysiol.* 40: 136–155, 1977.

FERSTER, D. Orientation selectivity of synaptic potentials in cat primary visual cortex. *J. Neurosci.* 6: 1284–1301, 1986.

FERSTER, D. Spatially opponent excitation and inhibition in simple cells of the cat visual cortex. *J. Neurosci.* 8: 1172–1180, 1988.

FERSTER, D., CHUNG, S., AND WHEAT, H. S. Orientation selectivity of synaptic input from the lateral geniculate nucleus to simple cells of the cat visual cortex. *Nature* 380: 249–252, 1995.

FERSTER, D. AND JAGADEESH, B. Nonlinearity of spatial summation in simple cells of areas 17 and 18 of cat visual cortex. *J. Neurophysiol.* 66: 1667–1679, 1991.

FERSTER, D. AND JAGADEESH, B. EPSP-IPSP interactions in cat visual cortex studied with in vivo whole-cell patch recording. *J. Neurosci.* 12: 1262–1274, 1992.

FERSTER, D. AND LINDSTRÖM, S. An intracellular analysis of geniculocortical connectivity in area 17 of the cat. *J. Physiol. (Lond.)* 342: 181–215, 1983.

GANZ, L. AND FELDER, R. Mechanism of direction selectivity in simple neurons of the cat's visual cortex analyzed with stationary flashed sequences. *J. Neurophysiol.* 51: 294–324, 1984.

GOODWIN, A. W., HENRY, G. H., AND BISHOP, P. O. Direction selectivity of simple striate cells: Properties and mechanisms. *J. Neurophysiol.* 38: 1500–1523, 1975.

GRZYWACZ, N. M. AND KOCH, C. Functional properties of models for direction selectivity in the retina. *Synapse* 1: 417–434, 1987.

HEEGER, D. J. Nonlinear model of cat striate physiology. *Vis. Neurosci.* 9: 181–197, 1992.

HEGGELUND, P. Quantitative studies of enhancement and suppression zones in the receptive field of simple cells in cat striate cortex. *J. Physiol. (Lond.)* 373: 293–310, 1986.

HOCHSTEIN, S. AND SHAPLEY, R. M. Quantitative analysis of retinal ganglion cell classifications. *J. Physiol. (Lond.)* 262: 237–264, 1976.

HUBEL, D. H. AND WIESEL, T. N. Receptive fields, binocular interaction and functional architecture in the cat's visual cortex. *J. Physiol. (Lond)*. 160: 106–154, 1962.

JAGADEESH, B., WHEAT, H. S., AND FERSTER, D. Linearity of summation of synaptic potentials underlying direction selectivity in simple cells of the cat visual cortex. *Science* 262: 1901–1904, 1993.

KOCH, C., DOUGLAS, R., AND WEHMEIER, U. Visibility of synaptically induced conductance changes: theory and simulations of anatomically characterized cortical pyramidal cells. *J. Neurosci.* 10: 1728–1744, 1990.

KOCH, C. AND POGGIO, T. Multiplying with synapses and neurons. In: *Single Neuron Computation.* New York: Academic, 1992, p. 315–345.

KOCH, C., POGGIO, T., AND TORRE, V. Retinal ganglion cells: a functional interpretation of dendritic morphology. *Philos. Trans. R. Soc. Lond. B Biol. Sci.* 298: 227–264, 1982.

KONTSEVICH, L. L. The nature of the inputs to cortical motion detectors. *Vision Res.* 35: 2785–2793, 1995.

MAEX, R. and ORBAN, G. A. Model circuit of spiking neurons generating directional selectivity in simple cells. *J. Neurophysiol.* 75: 1515–1545, 1996.

MCLEAN, J. AND PALMER, L. A. Contribution of linear spatiotemporal receptive field structure to velocity selectivity of simple cells in area 17 of the cat. *Vision Res.* 29: 675–679, 1989.

MCLEAN, J., RAAB, S., AND PALMER, L. A. Contribution of linear mechanisms to the specification of local motion by simple cells in areas 17 and 18 of the cat. *Vis. Neurosci.* 11: 295–306, 1994.

MOVSHON, J. A., THOMPSON, I. D., AND TOLHURST, D. J. Spatial summation in the receptive fields of simple cells in the cat's striate cortex. *J. Physiol. (Lond.)* 283: 53–77, 1978.

PALMER, L. A. AND DAVIS, T. L. Receptive-field structure in cat striate cortex. *J. Neurophysiol.* 46: 260–276, 1981.

POGGIO, T. AND REICHARDT, W. E. Considerations on models of movement detection. *Kybernetik* 13: 223–227, 1973.

REICHARDT, W. Autocorrelation, a principle for the evaluation of sensory information by the central nervous system. In: *Sensory Communication.* New York: Wiley, 1961.

REID, R. C., SOODAK, R. E., AND SHAPLEY, R. M. Linear mechanisms of direction selectivity in simple cells of cat striate cortex. *Proc. Natl. Acad. Sci. USA* 84: 8740–8744, 1987.

REID, R. C., SOODAK, R. E., AND SHAPLEY, R. M. Directional selectivity and spatiotemporal structure of receptive fields of simple cells in cat striate cortex. *J. Neurophysiol.* 66: 505–529, 1991.

SAUL, A. B. AND HUMPHREY, A. L. Evidence of input from lagged cells in the lateral geniculate nucleus to simple cells in cortical area 17 of the cat. *J. Neurophysiol.* 68: 1190–1208, 1992a.

SAUL, A. B. AND HUMPHREY, A. L. Temporal-frequency tuning of direction selectivity in cat visual cortex. *Vis. Neurosci.* 8: 365–372, 1992b.

SHAPLEY, R. AND LENNIE, P. Spatial frequency analysis in the visual system. *Annu. Rev. Neurosci.* 8: 547–583, 1985.

SILLITO, A. M. Inhibitory processes underlying the directional specificity of simple, complex and hypercomplex cells in the cat's visual cortex. *J. Physiol. (Lond.)* 271: 699–720, 1977.

SPITZER, H. AND HOCHSTEIN, S. Simple- and complex-cell response dependences on stimulation parameters. *J. Neurophysiol.* 53: 1244–1265, 1985.

STUART, G. J. AND SAKMANN, B. Active propagation of somatic action potentials into neocortical pyramidal cell dendrites. *Nature* 367: 69–72, 1994.

TOLHURST, D. J. AND DEAN, A. F. Evaluation of a linear model of directional selectivity in simple cells of the cat's striate cortex. *Vis. Neurosci.* 6: 421–428, 1991.

TORRE, V. AND POGGIO, T. A synaptic mechanism possibly underlying direction selectivity to motion. *Proc. R. Soc. Lond. Ser. B* 202: 409–416, 1978.

VAN SANTEN, J.P.H. AND SPERLING, G. Temporal covariance model of human motion detection. *J. Opt. Soc. Am.* 1: 451–473, 1984.

WATSON, A. B. AND AHUMADA, A. J. A look at motion in the frequency domain. In: *Motion: Perception and Representation.* New York: Association for Computing Machinery, 1983.

WATSON, A. B. AND AHUMADA, A. J. Model of human visual-motion sensing. *J. Opt. Soc. Am.* 2: 322–341, 1985.

WOLMANN, D. E. AND PALMER, L. A. The effects of GABA blockade on the spatiotemporal structure of neurons in cat striate cortex (Abstract). *Invest. Ophthalmol. Vis. Sci. (Suppl.)* 34: 908, 1993.